

University of Alberta

Robust matrix rank reduction methods for seismic data processing

by

Ke Chen

A thesis submitted to the Faculty of Graduate Studies and Research
in partial fulfillment of the requirements for the degree of

Master of Science
in
Geophysics

Department of Physics

©Ke Chen
Fall 2013
Edmonton, Alberta

Permission is hereby granted to the University of Alberta Libraries to reproduce single copies of this thesis and to lend or sell such copies for private, scholarly or scientific research purposes only. Where the thesis is converted to, or otherwise made available in digital form, the University of Alberta will advise potential users of the thesis of these terms.

The author reserves all other publication and other rights in association with the copyright in the thesis and, except as herein before provided, neither the thesis nor any substantial portion thereof may be printed or otherwise reproduced in any material form whatsoever without the author's prior written permission.

To my parents and all my teachers

Abstract

An important step of seismic data processing entails signal de-noising. Traditional de-noising methods assume Gaussian noise model and their performance degrades in the presence of erratic (non-Gaussian) noise. This thesis examines the problem of designing reduced-rank noise attenuation algorithms that are resistant to erratic noise.

I first introduce a robust matrix factorization based on M-estimate and incorporate it into the formulation of the classical Singular Spectrum Analysis (SSA) algorithm. This new algorithm (Robust SSA) permits to de-noise seismic data that have been contaminated by non-Gaussian noise.

I also propose a second Robust SSA algorithm that attacks the data de-noising and reconstruct problems as low-rank matrix recovery problem that is solved by a convex optimization algorithm. The NP-hard rank minimization problem is replaced by its tightest convex relaxation, the nuclear-norm minimization. An augmented Lagrangian method is used to numerically look for the solution that minimizes the cost function.

Acknowledgements

First and foremost, I thank my supervisor, Dr. Mauricio Sacchi. His passion for geophysics research has deeply influenced me. His patience and encouragement are important for me for completing this MSc degree. I feel honoured to be a part of the Signal Analysis and Imaging Group (SAIG) consortium for my MSc study and research. I thank my supervisor for forming this group and the consortium sponsors for providing financial support. I would like to thank my colleagues at the SAIG for scientific discussions as well as friendships. I thank the friends I made in the University of Alberta for making life here enjoyable. In particular, I would like to thank my examining committee, Dr. Claire Currie, Dr. Mathieu Dumberry and Dr. Yu Gu, for taking their time to read and providing valuable suggestions on my thesis. Finally, I thank my parents for their sustaining encouragement and support on my journey of overseas study.

Contents

1	Introduction	1
1.1	Background	1
1.2	Seismic noise	3
1.3	Seismic noise attenuation methods	4
1.3.1	Random seismic noise attenuation	5
1.3.2	Erratic seismic noise attenuation	8
1.4	Seismic data reconstruction methods	10
1.5	Motivations	12
1.6	Organization of this thesis	12
2	SSA and its applications in seismic data processing	14
2.1	Introduction	14
2.2	Review of multivariate statistics	15
2.2.1	Random variable (univariate)	15
2.2.2	Random vector (multivariate)	16
2.2.3	Population mean, population variance, population covariance and population correlation coefficient	17
2.2.4	Complex random variable	20
2.2.5	Sample mean, sample variance, sample covariance, sample correlation coefficient	22
2.2.6	Eigendecomposition	24

2.2.7	Principal component analysis	25
2.3	Theory of SSA	32
2.3.1	Dynamical system	32
2.3.2	Embedding into a trajectory matrix	34
2.3.3	Trajectory matrix decomposition	34
2.3.4	Rank reduction and Eigenimage grouping	38
2.3.5	Time series reconstruction	39
2.4	SSA for time series analysis	40
2.5	Applications of SSA in seismic data processing	44
2.5.1	Signal model in Fourier domain	44
2.5.2	Embedding	48
2.5.3	Decomposition	49
2.5.4	Rank reduction	49
2.5.5	Anti-diagonal averaging	50
2.5.6	Inverse Fourier transform	50
2.5.7	Examples	50
2.6	Summary	52
3	Robust SSA	60
3.1	Introduction	60
3.2	Review of robust statistics	61
3.2.1	Location estimation	62
3.2.2	Scale estimation	63
3.2.3	Linear regression	64
3.3	M-estimate method	66
3.3.1	M-estimates of location	67
3.3.2	A weighted least-squares view	69
3.3.3	Scale equivariant M-estimate of location	69

3.3.4	Auxiliary step: M-estimate of scale	72
3.3.5	Iteratively reweighted least-squares	73
3.3.6	Loss function ρ , ψ function and weight function	74
3.4	Robust SSA	78
3.4.1	Robust low rank approximation	78
3.5	Examples	82
3.5.1	t - x domain robust rank reduction	82
3.5.2	Synthetic Example	84
3.5.3	Field Data Example	87
3.6	Summary	90
4	Nuclear-norm minimization	98
4.1	Introduction	98
4.2	Theory	99
4.2.1	Notation	99
4.2.2	Singular spectrum analysis	99
4.2.3	Low-rank matrix recovery	100
4.2.4	Augmented Lagrangian method	102
4.2.5	Parameter Selection and Stopping Criterion	104
4.3	Examples	105
4.3.1	Synthetic Example 1	105
4.3.2	Synthetic Example 2	108
4.4	Summary	110
5	Conclusions	112
	Bibliography	114
	Appendices	
A	Gradient in Complex Domain	123

List of Figures

1.1	A simple sketch map of 2-D seismic survey (one flat layer). Red star represents source, blue triangle represents receivers, dash line represents ray path, and M is midpoint. a) Shot-receiver coordinates. b) Midpoint-offset coordinates. .	2
1.2	A shot gather from a 2-D seismic survey in Alberta.	3
2.1	Geometric interpretation of population PCA, a 2-variate example. $\mathbf{x}_1, \mathbf{x}_2$ are the original random variable, also the original coordinate axes; \mathbf{w}_1 and \mathbf{w}_2 are the principal components, also the new coordinate axes. $\mathbf{w}_1 = \mathbf{u}_1^T \mathbf{X} = u_{11}\mathbf{x}_1 + u_{21}\mathbf{x}_2$, $\mathbf{w}_2 = \mathbf{u}_2^T \mathbf{X} = u_{12}\mathbf{x}_1 + u_{22}\mathbf{x}_2$. The ellipse is defined by the population covariance matrix \mathbf{C} and constant c , which can represent a constant probability density contour of \mathbf{X}	29
2.2	Geometric interpretation of sample PCA, a 2-variate example. $\mathbf{x}_1, \mathbf{x}_2$ are the original random variable, also the original coordinate axes; \mathbf{w}_1 and \mathbf{w}_2 are the sample principal components, also the new coordinate axes. $\mathbf{w}_1 = \mathbf{u}_1^T \mathbf{X} = u_{11}\mathbf{x}_1 + u_{21}\mathbf{x}_2$, $\mathbf{w}_2 = \mathbf{u}_2^T \mathbf{X} = u_{12}\mathbf{x}_1 + u_{22}\mathbf{x}_2$. \mathbf{u}_1 and \mathbf{u}_2 are the eigenvectors of the sample covariance matrix \mathbf{S} . The asterisks represent 200 data samples drawn from multivariate Gaussian distribution with covariance matrix \mathbf{C} and zero mean. The ellipse is defined by the sample covariance matrix \mathbf{S} and constant c	33
2.3	Southern Oscillation Index (SOI) from January 1876 to July 2013.	41
2.4	The singular spectrum of trajectory matrix of Southern Oscillation Index. There are six leading singular values and remaining smaller singular values. .	42
2.5	Six leading eigenvectors of the covariance matrix. From top to bottom, the eigenvalues corresponding the eigenvectors decrease. These transformation bases are derived from the data itself.	42
2.6	Six principal components. They are the projection of trajectory matrix onto eigenvectors 1 - 6, respectively.	43
2.7	Six reconstructed time series by eigenimages 1-6, respectively.	43
2.8	Original SOI time series (black line) and reconstructed time series by first 4 eigenimages (red line).	44

2.9	The predictable property of linear events in f - x domain. a) A seismic section consists of one single linear event in t - x domain. b) Amplitude spectra of the t - x data. c) The real part of the data in f - x domain. d) The real part of the complex Fourier coefficient at 20 Hz.	46
2.10	a) Noise-free seismic data section consists of three linear events. b) The singular spectra of the trajectory matrices constructed from different frequency slices. c) The real part of the frequency slice at 10 Hz. d) The singular spectrum of the trajectory matrix constructed from frequency slice at 10 Hz.	53
2.11	a) Noise-free data after SSA filtering. b) Noise-free data after f - x deconvolution filtering. c) Difference between noise-free data and SSA filtered data. d) Difference between noise-free data and f - x deconvolution filtered data.	54
2.12	a) Seismic data section consists of three linear events, corrupted with Gaussian noise (SNR=1). b) The singular spectra of the trajectory matrices constructed from different frequency slices. c) The real part of the frequency slice at 10 Hz. d) The singular spectrum of the trajectory matrix constructed from frequency slice at 10 Hz.	55
2.13	a) Data corrupted with Gaussian noise after SSA filtering. b) Data corrupted with Gaussian noise after f - x deconvolution filtering. c) Difference between noisy data and SSA filtered data. d) Difference between noisy data and f - x deconvolution filtered data.	56
2.14	a) Seismic data section consists of three linear events, corrupted with Gaussian noise (SNR=1) and erratic noise. b) The singular spectra of the trajectory matrices constructed from different frequency slices. c) The real part of the frequency slice at 10 Hz. d) The singular spectrum of the trajectory matrix constructed from frequency slice at 10 Hz.	57
2.15	a) Data corrupted with Gaussian noise and erratic noise after SSA filtering. b) Data corrupted with Gaussian noise and erratic noise after f - x deconvolution filtering. c) Difference between noisy data and SSA filtered data. d) Difference between noisy data and f - x deconvolution filtered data.	58
2.16	a) Data corrupted with Gaussian noise and erratic noise after robust SSA filtering. b) Difference between noisy data and robust SSA filtered data. c) Real part of the frequency slice at 10 Hz of the robust SSA filtered data. d) Singular spectrum of the frequency slice at 10 Hz of the robust SSA filtered data.	59
3.1	Gaussian distributed samples (black solid circles), population mean (green five-pointed star), the sample mean (red arrow below axis) and sample median (blue arrow below axis) of 14 “clean” samples, the sample mean (red arrow above axis) and sample median (blue arrow above axis) of 15 samples containing one outlier.	63
3.2	Three loss functions. Quadratic function, Huber function and Biweight function. τ_H is the tuning constant in Huber function, τ_B is the tuning constant in biweight function.	75

3.17	The comparison of error panels of three different methods in the right rectangular window. Error panels of f - x deconvolution (a), SSA (b), and robust SSA (c).	94
3.18	Field data example from Alaska. (a) Poststack data with erratic noise. (b) Data filtered by f - x deconvolution. (c) Data filtered by SSA. (d) Data filtered by robust SSA.	95
3.19	Error panels of (a) f - x deconvolution, (b) SSA, (c) robust SSA.	96
3.20	Zoomed sections correspond to the rectangular window. (a) Original data with erratic noise. (b) Data filtered by f - x deconvolution. (c) Data filtered by SSA. (d) Data filtered by robust SSA. (e) Error panel of f - x deconvolution. (f) Error panel of SSA. (g) Error panel of robust SSA.	97
4.1	(a) Synthetic seismic data with 50% traces missing and 5 traces corrupted with erratic noise. b) Data filtered by robust SSA via low-rank matrix recovering. (c) Sparse erratic noise obtained from robust SSA. (d) Noise-free synthetic data. (e) Difference section between noise-free synthetic data and data filtered by robust SSA.	108
4.2	(a) Synthetic seismic data with 25% traces missing, Gaussian noise (SNR=2) and 5 traces corrupted with erratic noise. b) Data filtered by robust SSA via low-rank matrix recovering. (c) Sparse erratic noise obtained from robust SSA. (d) Noise-free synthetic data. (e) Difference section between noise-free synthetic data and data filtered by robust SSA.	111

CHAPTER 1

Introduction

1.1 Background

Exploration geophysics is an interdisciplinary science involved with physics, mathematics, and geology. It utilizes geophysical data observed on the surface of the earth to measure and then invert for physical properties of the subsurface. The aim is to explore minerals, hydrocarbons, groundwater reservoirs without the need to directly penetrate the earth's interior. Different geophysical methods can be used for "imaging" subsurface structures, e.g. seismic methods, gravitational methods, electrical methods, magnetic and electromagnetic methods. The seismic method is often used in the exploration of hydrocarbons. In this dissertation, I will mainly focus on problems in exploration seismology.

In a *seismic experiment*, a controlled seismic source excites the earth and generates impulsive sound waves that travel in the earth's interior. The waves propagate through the earth, part of them are attenuated in the earth's interior, part of them are reflected back when they reach geological boundaries. The reflected data are recorded by the receivers (geophones) deployed on the earth's surface. This is the first step of exploration seismology, known as *data acquisition*. The simplest acquisition configuration is to deploy a source and receivers along a line (Figure 1.1 (a)). The latter is referred to as 2-D seismic survey. The source is fired and the seismograms are recorded by the receivers. The seismograms recorded at different receivers are grouped together in one *common shot gather*. Then, the whole acquisition system is moved along the line to the next position to repeat experiment, and so on. The data acquisition is in shot-receiver coordinate system. While, many seismic processing sequences are applied in midpoint-offset coordinate system (Figure 1.1 (b)). The recorded seismic traces with the same mid-point location can be grouped together as a common mid-point (CMP) gather. A shot gather from Yilmaz's data set (shot 25 in the

book *Seismic Data Analysis*) is shown in Figure 1.2. This shot gather is from a 2-D land survey in Alberta, Canada. The survey uses a split-spread geometry where the source is located in the center of receiver cable. Different waves are observed including direct waves, refractions and reflections as indicated in Figure 1.2. The exploration method that uses refractions is known as the *refraction method* and it is often used for near surface studies and for crustal studies. The exploration, development and monitoring of reservoirs of oil and gas is mainly carried out via reflected waves with the *reflection method*.

Recorded seismic wavefields are often contaminated by coherent and incoherent noise. Several types of noise are presented in Figure 1.2, coherent noise such as ground roll, high-amplitude erratic (non-Gaussian) noise and the ambient random noise presents in the whole section.

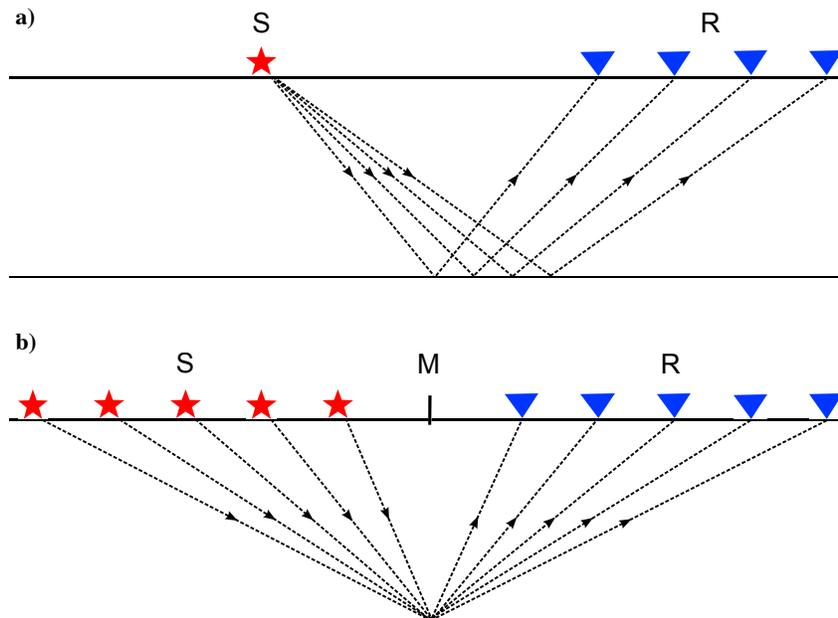


Figure 1.1: A simple sketch map of 2-D seismic survey (one flat layer). Red star represents source, blue triangle represents receivers, dash line represents ray path, and M is midpoint. a) Shot-receiver coordinates. b) Midpoint-offset coordinates.

The second step in the reflection seismology is called *data processing*. In this step the collected data are processed and analyzed via mathematical and physical principles. In the *interpretation* step, the processed data and images are interpreted as geological structures to indicate the location of potential oil and gas reservoir. The seismic data processing can be divided to three principal steps: *deconvolution*, *CMP stacking*, and *migration*. Deconvolution removes the seismic wavelet from the seismic data to broaden the frequency band

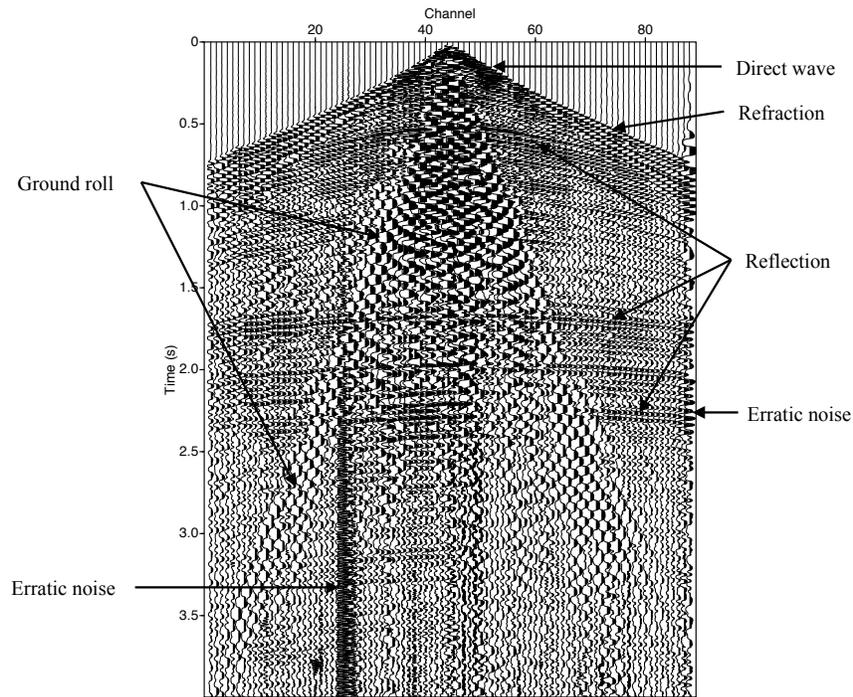


Figure 1.2: A shot gather from a 2-D seismic survey in Alberta.

of the data. In other words, deconvolution is used to improve temporal resolution. CMP stacking averages NMO corrected seismic traces in each CMP gather along offset dimension to estimate a zero-offset seismic section. It can suppress both random noise and coherent noise to improve the signal-to-noise ratio of seismic data. Migration is an imaging process that moves dipping events to their true subsurface positions. There are many other auxiliary processes that are often run in between each one of the three main processes. This thesis will study noise suppression and missing data reconstruction via reduce-rank methods. This is a step that should be carried out before or after stacking and prior to migration. Noise suppression can also be carried out in different domains.

1.2 Seismic noise

In exploration seismology, one wants to keep reflections and eliminate coherent and incoherent noise (Yilmaz, 2001). *Incoherent noise*, as its name implies, is not correlated from trace to trace. That is to say, the phase of the noise is independent between adjacent traces. Incoherent noise is also known as *random noise*. It can be caused by a variety of factors such as wind, human and animal activity, rain drops, instrumental noise, etc.

1999). In this particular domain, the coefficients corresponding to noise are eliminated while the remaining coefficients are inverted back to the original domain. One can also eliminate the coefficients corresponding to the signal and keep those associated with noise. The latter permits an estimation of a model of the noise that can be subtracted from the original data.

1.3.1 Random seismic noise attenuation

Many methods for random noise attenuation have been developed in the past several decades. First, *CMP stacking* (Mayne, 1962) was propose to reduce random noise by averaging NMO corrected seismic traces with different offsets in each common mid-point gather. There are processes that require suppressing noise prior to stacking or to apply noise suppression after stacking. This is why our arsenal of seismic processing algorithms often contains various methods for noise attenuation that can operate in different domains and with pre-stack and post-stack data.

Frequency band-pass filtering can be used for suppressing ambient noise by restricting the amplitude spectrum of the seismic data. However, signal and noise often overlap in the frequency domain and therefore, one might be eliminating a portion of the signal when applying frequency domain band-pass filtering.

Random noise reduction via *spatial prediction filtering* has been proposed as an alternative to frequency band-pass filtering. The prediction filters can be estimated and applied in the $f-x$ domain or $t-x$ domain. The principle in this type of filters resides on the lateral predictability of signals. Canales (1984) firstly proposed the $f-x$ prediction technique for seismic random noise reduction. This method assumes that noise-free seismic signal is composed of linear or nearly linear events in $t-x$ domain. For one particular frequency slice in $f-x$ domain, the signal is the superposition of a finite number of complex exponentials. The Fourier coefficients of one particular frequency from different traces are linearly dependent with each other. Therefore, some of the Fourier coefficients can be predicted from others, i.e. $f-x$ signal is linear predictable in space. This method implicitly assumes that the $f-x$ domain seismic data can be represented by the autoregressive (AR) model, i.e. the linearly predictable part is the signal and the unpredictable portion is the white noise. The prediction error filter (PEF) is firstly estimated from the data, and then the noise is estimated via applying the PEF on the data. Gulunay (1986) named this technique as $f-x$ deconvolution. The $f-x$ deconvolution is known to damage original signal if the noise level is high, i.e. it cannot separate the signal and noise perfectly. One of the reasons is that it uses the biased autocorrelation method that assumes the data outside the window are zero. Harris and White (1997) propose to use the transient-free data matrix to alleviate this problem (Ulrych and Clayton, 1976). The other reason is that, the data in $f-x$ actually does not follow the AR

This method is equivalent to using zero-lag covariance matrix after flattening the events via linear moveout correction. Finally, a reverse linear moveout correction is applied after the zero-lag K-L filtering. Besides, they discuss about using K-L transform to remove multiples in CMP gather. The multiples are flattened by NMO correction and primary events are under-corrected or over-corrected. The multiples correspond to the largest eigenvalues and primaries correspond to smaller eigenvalues. Marchisio et al. (1988) applied the full K-L transform that has all lags (temporal and spatial), and also the partial K-L transform that has fewer time lags in the covariance matrix for random noise attenuation and VSP wavefield separation. It works for data with dipping events. Al-Yahya (1991) proposes the partial K-L transform for incoherent noise attenuation in the situation that there are several conflict dips in the seismic section. It is an extension of Jones and Levy (1987)'s method. For each dipping event, it is flattened by the linear moveout correction and a zero-lag K-L filtering is followed. The inverse linear moveout correction is applied on the filtered data. This procedure is repeated for all the dipping events and the results are summed. Freire and Ulrych (1988) applied singular value decomposition (SVD) in $t-x$ domain to separate the upgoing and downgoing wavefield in vertical seismic profiling (VSP) data. They also discussed the relationship between the SVD and the K-L transform. Ulrych et al. (1988) discussed several applications of SVD for reflection seismic data processing such as signal to noise enhancement, dip filtering, separation of upgoing and downgoing wavefield in VSP data and residual static correction. They referred to this technique as eigenimage reconstruction. The $t-x$ domain eigenimage approach has the advantages that the regular sampling in time or space direction is not necessary and it's free of aliasing problems. Liu (1999) and Chiu and Howell (2008) and Cary and Zhang (2009) applied the K-L transform or SVD for ground roll attenuation.

The above $t-x$ domain rank reduction methods need linear move-out correction when dealing with dipping events. Mars et al. (1987) applied the spectral matrix filtering for seismic random noise attenuation in CDP gather. They also used a synthetic example to show that spectral matrix filtering can be used for wavefield separation. Mari and Glangeaud (1990) applied the spectral matrix filtering for signal-to-noise ratio enhancement in VSP seismic data, and for wavefield separation in VSP seismic data. It works in $f-x$ domain and the K-L transform is applied on a constructed spectral matrix. Trickett (2003) proposed the $f-xy$ eigenimage filtering for random noise reduction in stacked 3D seismic volumes. It conducts rank reduction on each 2-D constant-frequency slice, which works well for dipping events. Trickett (2002) introduced Cadzow's algorithm for random seismic noise attenuation on 2-D seismic section as an alternative to $f-x$ prediction methods. He called it $f-x$ eigenimage filtering. Trickett (2008) extended Cadzow's algorithm for seismic denoising to three or more dimensional seismic data. He modified the name of the algorithm as Cadzow filtering. Trickett et al. (2010) proposed to use Cadzow's algorithm for seismic data re-

robust SSA involves a low-rank matrix recovery problem. It looks for the low-rank component from the incomplete and Gaussian and non-Gaussian (impulsive) noise corrupted data matrix. The NP-hard rank minimization problem is approximated by its tightest convex relaxation, the nuclear norm minimization problem. It changes the non-convex optimization problem to convex one. An augmented Lagrangian method is used for numerically solving the optimization problem. A synthetic example is shown to evaluate the performance of the proposed algorithm.

- Chapter 5 gives the summary and conclusions of the thesis. Moreover, future work is discussed.

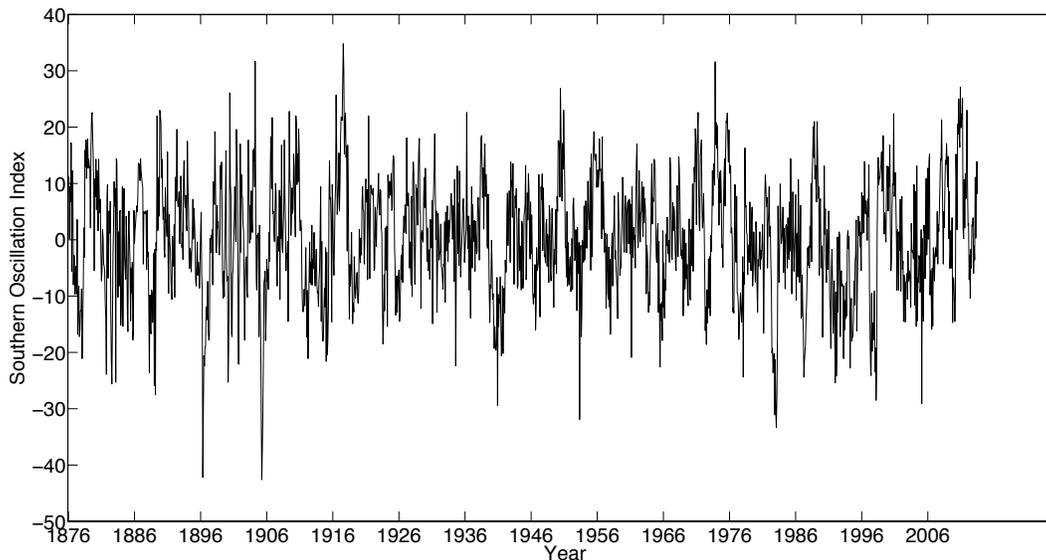


Figure 2.3: Southern Oscillation Index (SOI) from January 1876 to July 2013.

That is to say, some anharmonic oscillations may need many Fourier bases (harmonics) to be represented but only a few eigenvectors in SSA. Figure 2.6 shows the principal components 1 to 6 of the trajectory matrix. They were computed by projecting the trajectory matrix onto eigenvectors 1 to 6, respectively. That is to say, the i th principal component is given by $\mathbf{w}_i^T = \mathbf{u}_i^T \mathbf{M}$. \mathbf{u}_i^T is the i th eigenvector of the covariance matrix \mathbf{S} and \mathbf{M} is the trajectory matrix. Principal components 1 and 2 are similar in shape, they have a period of about 4 years. Principal components 3 and 4 are similar in shape, their period are about 2 years. Figure 2.7 shows the time series reconstructed from eigenimages 1 to 6, respectively. That is to say, the i th reconstructed time series is given by Equation (2.96) with eigenimage $\mathbf{M}_k = \mathbf{M}_i = \sigma_i \mathbf{u}_i \mathbf{v}_i^T$. Reconstructed time series 5 displays a nonlinear trend and an oscillatory component. The oscillation patterns in the reconstructed time series 6 (or principal component 6) is dominated by oscillatory noise. The signal-to-noise ratio enhanced SOI time series are reconstructed by adding the first 4 reconstructed time series (Figure 2.8). We can find that the reconstructed time series captures most of the oscillation behaviour of the time series with a reduction of noise.

where ω is frequency, complex coefficient $A(\omega)$ is the Fourier transform of the wavelet $a(t)$. Assume that the spatial interval between traces is regular, $x = (j - 1)\Delta x$, $j = 1, 2, \dots, N$ is the trace index in the spatial axis and Δx is the spatial interval between two adjacent traces. Here, we use $j - 1$ to indicate that the first trace has zero offset. The Fourier coefficient at frequency ω of j th trace is

$$D(\omega, (j - 1)\Delta x) = A(\omega)e^{-i\omega p(j-1)\Delta x}. \quad (2.99)$$

To be more convenient, we note $D_j(\omega) = D(\omega, (j - 1)\Delta x)$

$$D_j(\omega) = A(\omega)e^{-i\omega p(j-1)\Delta x}, \quad (2.100)$$

The Fourier coefficient at frequency ω at trace $j - 1$ is

$$D_{j-1}(\omega) = A(\omega)e^{-i\omega p(j-2)\Delta x} = A(\omega)e^{-i\omega p(j-1)\Delta x}e^{i\omega p\Delta x} = e^{i\omega p\Delta x}D_j(\omega), \quad (2.101)$$

In other words, there is a linear recursion relationship between adjacent traces

$$D_j(\omega) = PD_{j-1}(\omega), \quad (2.102)$$

where $P = e^{-i\omega p\Delta x}$. The linear predictable property of one single linear event in f - x domain is shown in Figure 2.9. The frequency slice of Fourier transform of seismic section consists of one single linear event is a complex harmonic. The real part of the frequency slice is a sinusoid (Figure 2.9(c)).

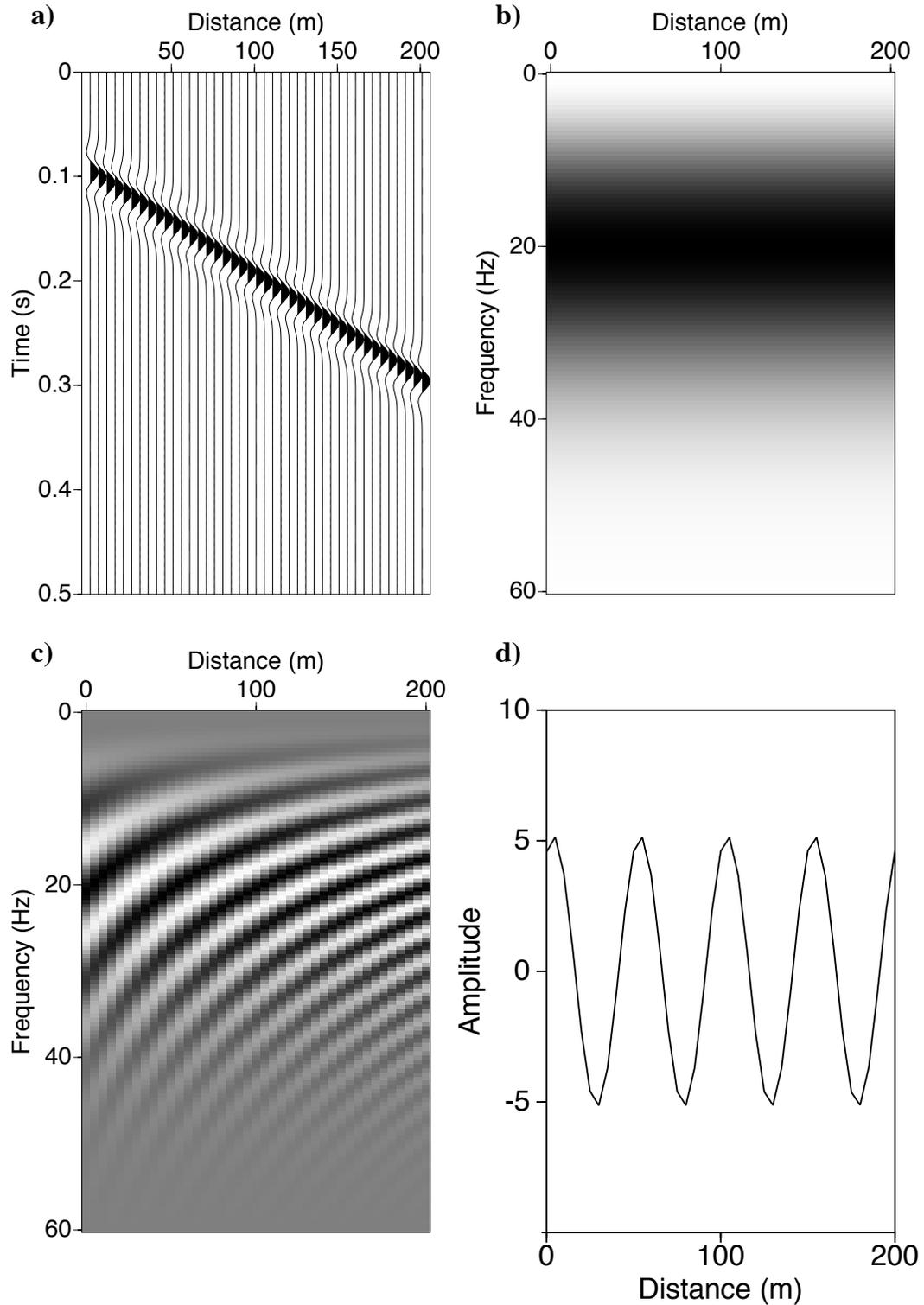


Figure 2.9: The predictable property of linear events in $f-x$ domain. a) A seismic section consists of one single linear event in $t-x$ domain. b) Amplitude spectra of the $t-x$ data. c) The real part of the data in $f-x$ domain. d) The real part of the complex Fourier coefficient at 20 Hz.

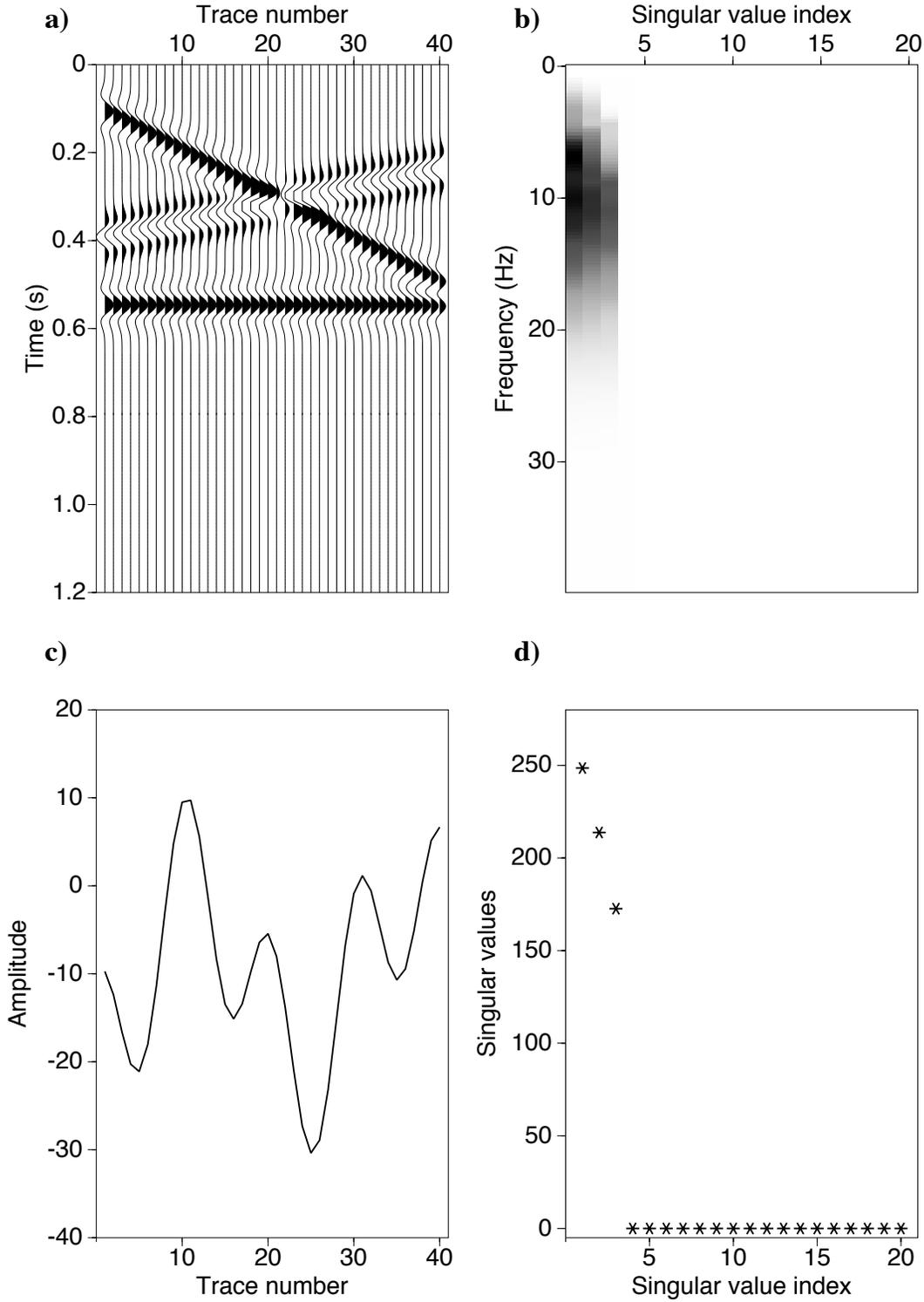


Figure 2.10: a) Noise-free seismic data section consists of three linear events. b) The singular spectra of the trajectory matrices constructed from different frequency slices. c) The real part of the frequency slice at 10 Hz. d) The singular spectrum of the trajectory matrix constructed from frequency slice at 10 Hz.

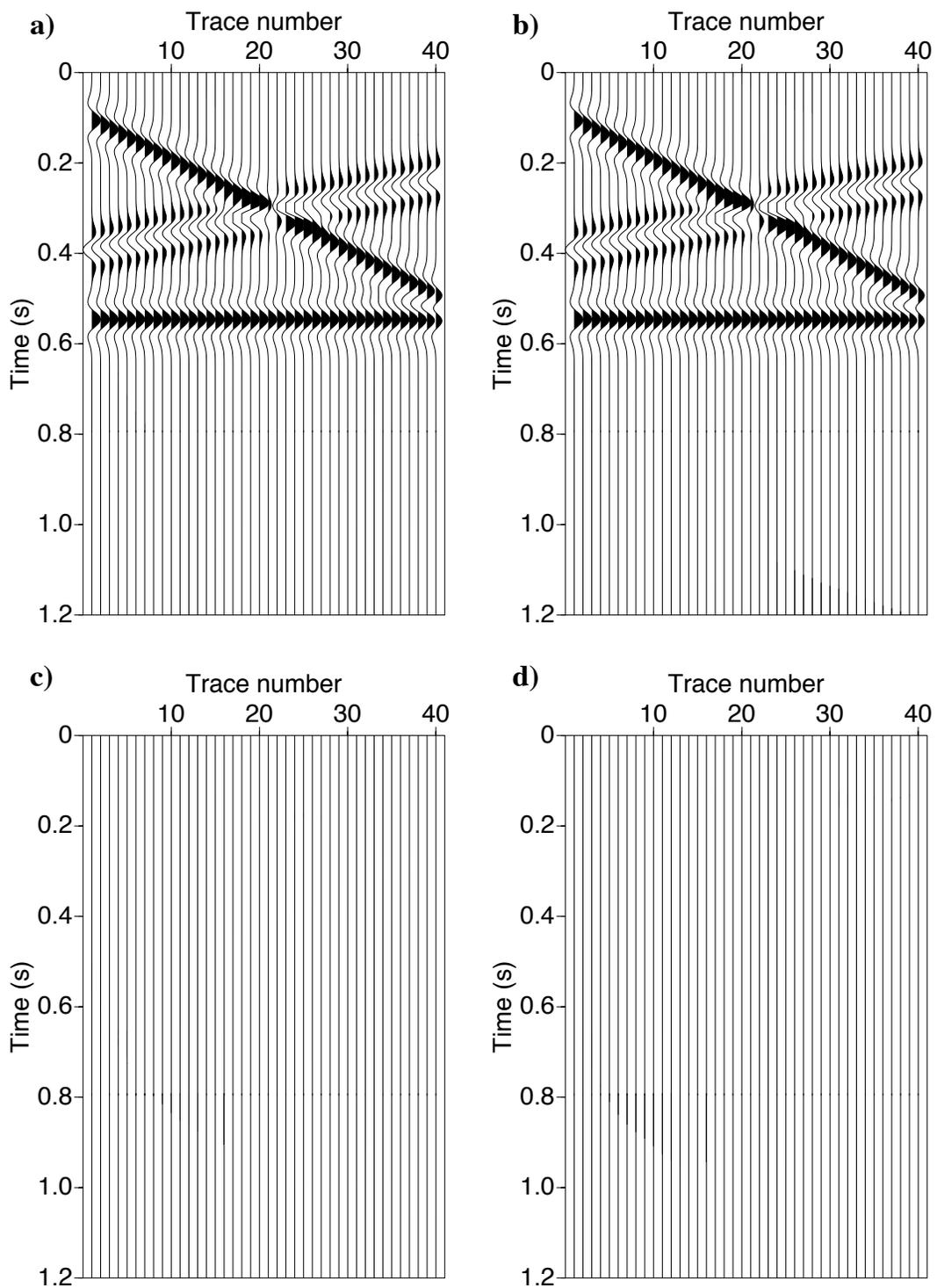


Figure 2.11: a) Noise-free data after SSA filtering. b) Noise-free data after $f-x$ deconvolution filtering. c) Difference between noise-free data and SSA filtered data. d) Difference between noise-free data and $f-x$ deconvolution filtered data.

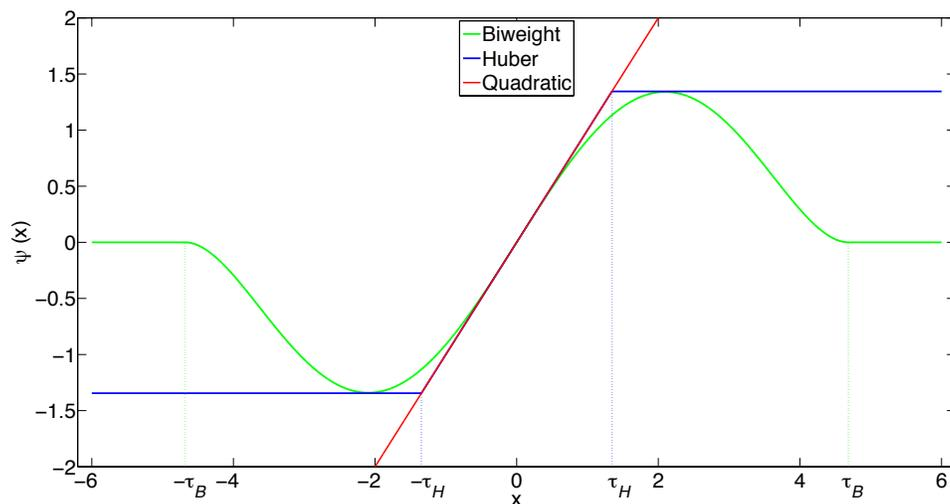


Figure 3.3: Three ψ functions corresponding to Quadratic function, Huber function and Biweight function. τ_H is the tuning constant in ψ function of Huber function, τ_B is the tuning constant in ψ function of biweight function.

The ψ functions are shown in Figure 3.3. ψ_Q and ψ_H are monotone functions, ψ_B is a “re-descending” function. ψ_Q is a linear function, ψ_H and ψ_B are nonlinear.

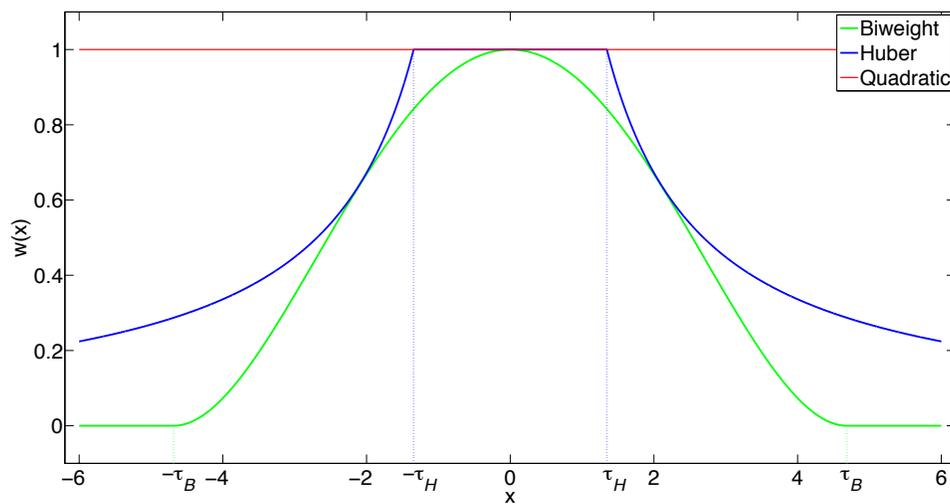


Figure 3.4: Weight functions corresponding to Quadratic function, Huber function and biweight function. τ_H is the tuning constant in weight function of Huber function, τ_B is the tuning constant in weight function of biweight function.

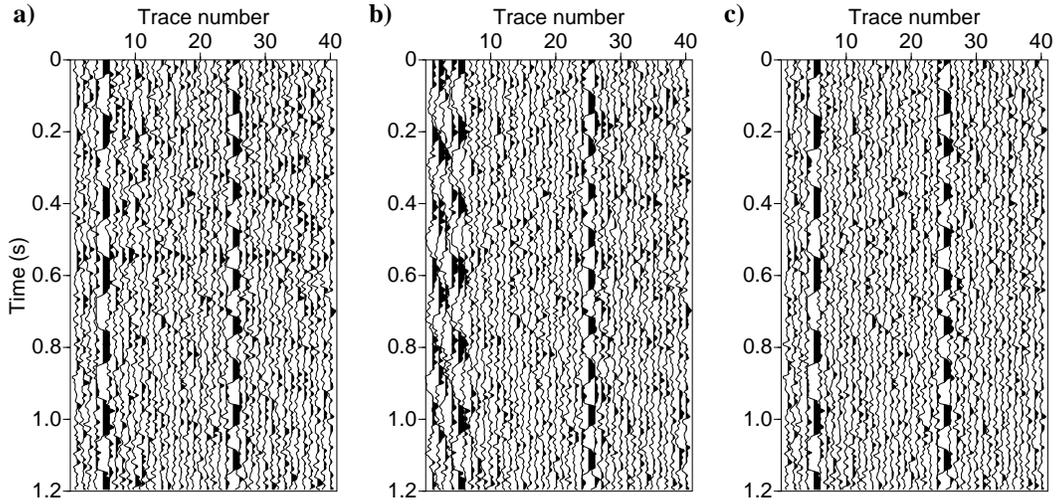


Figure 3.9: Error panels of f - x deconvolution (a), SSA (b), and robust SSA (c).

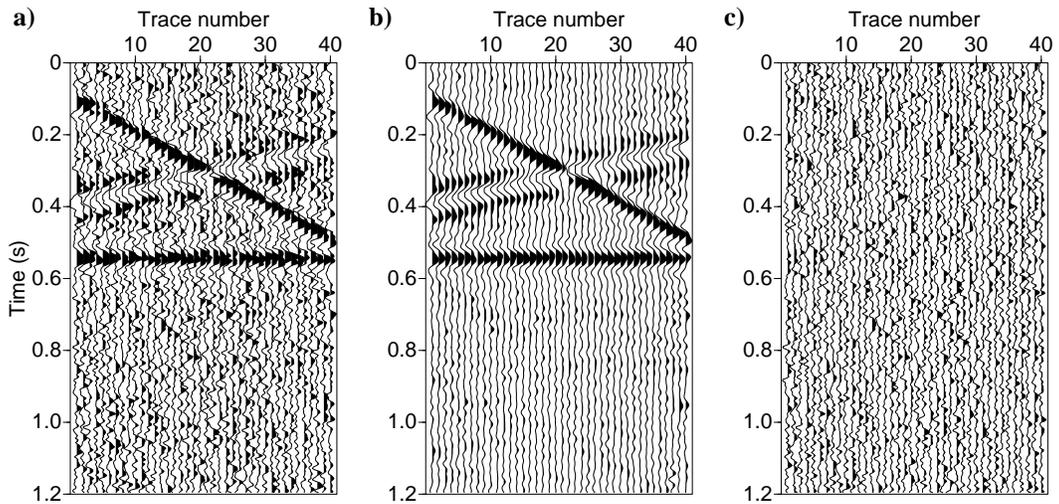


Figure 3.10: (a) Data corrupted with only Gaussian noise. (b) Data after classical SSA filtering. (c) Error panel of classical SSA.

3.5.3 Field Data Example

Western Canadian Sedimentary Basin

Figure 3.11(a) is a poststack data section from a survey in Western Canadian Sedimentary Basin. It has 800 traces and 1500 time samples with the time sample interval equals to 2 ms. Figure 3.11(b) and Figure 3.11(c) are the zoomed data section in the left and right rectangular windows highlighted in Figure 3.11(a), respectively. We can see high-amplitude noise in this data set. The whole data are divided into overlapped windows with suitable size. Then, all windows are filtered and added back to recover the clean data. In spatial direction, each window has 50 traces and the overlap between two adjacent windows is 25 traces. In temporal direction, each window has 300 samples (0.6 s) and the overlap between two adjacent windows is 100 samples (0.2 s). All the three filtering methods are applied for frequencies in the band of 1-80 Hz. The size of the reconstructed subspace in both SSA and robust SSA methods is set to be 2. The reason for choosing this rank is that the data are only a two dimensional data set and also the events in each small window are relatively flat. In robust SSA, the external iterations (for updating weights) is 10 and number of internal iterations (for alternating minimization) is 5. We set the tuning constant α for bisquare estimator as 3.3. We set the length of f - x prediction filter as 6 and the trade-off parameter as 0.001. We use the same parameters for the whole data set. Again, we compare the performance of f - x deconvolution, SSA and robust SSA on noise attenuation. To compare the results of three methods objectively, all the image plots (Figure 3.11(a), Figure 3.12, Figure 3.13) have been clipped to the same value. The wiggle plots corresponding to the left rectangular window (Figure 3.11(b), Figure 3.14) have been clipped to the same value. The error panels (Figure 3.15) have been clipped to another same value to better compare the details of the estimated noise of the three methods. Similarly, wiggle plots corresponding to the right rectangular window (Figure 3.11(c), Figure 3.16) have been clipped to the same value. The error panels (Figure 3.17) have been clipped to another same value. The results of the three methods applied on the whole data set are shown in Figure 3.12. Robust SSA suppresses much more high-amplitude erratic noise than f - x deconvolution and classical SSA. The comparison of error panels (Figure 3.13) shows that the f - x deconvolution leaks more signal energy into the noise section than robust SSA. We show the zoomed results for window to the left in Figure 3.11(a) as Figure 3.14. The results for window to the right of Figure 3.11(a) are shown in Figure 3.16. Robust SSA is more effective than f - x deconvolution and SSA. We can find that there are more details for deep layers appear after robust SSA filtering than the other two. The error panels (Figure 3.15, Figure 3.17) of the two particular windows highlighted in Figure 3.11(a) do not show obvious energy leakage of the signal. Note that the using of patching technique makes the estimation of f - x filters or least-squares singular vectors in one particular patch (e.g. shallower windows) not

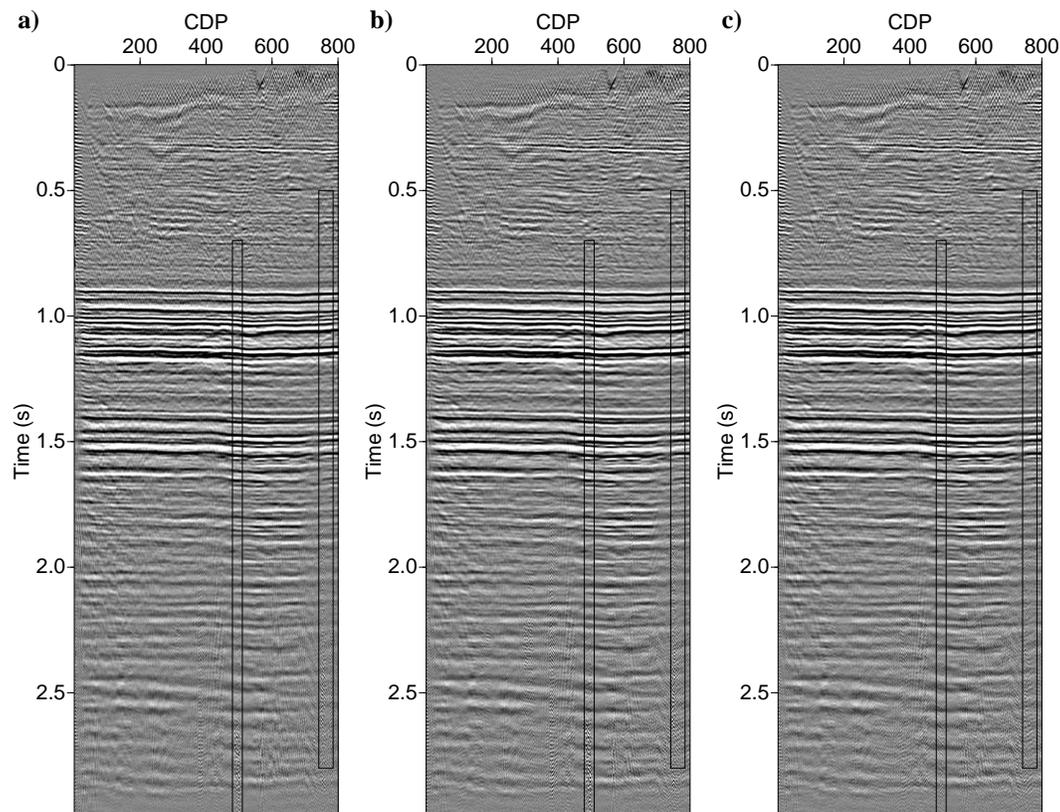


Figure 3.12: The comparison of the results of three different methods. (a) Data after f - x deconvolution filtering. (b) Data after classical SSA filtering. (c) Data after robust SSA filtering.

direction and, 300 time samples (0.6 s) with 75 overlapping samples (0.15 s) in temporal direction. The processing frequency band for all the three methods ranges from 1 to 60 Hz. The size of subspace of the reconstructed data is chosen to be $K = 3$ in both robust SSA and SSA. In robust SSA, the outer iteration (for reweighting) number is set to be 10 and the inner iteration (for alternating minimization) number is set to be 5. The tuning constant α for bisquare estimator used here is 4.2. The prediction length and trade-off parameter of f - x deconvolution are 8 and 0.001, respectively. The results of the f - x deconvolution, SSA and robust SSA are compared. All the image plots and wiggle plots are clipped to the same value to make the results are better compared. Robust SSA (Figure 3.18 (d)) thoroughly removes the high amplitude erratic noise. While, both f - x deconvolution (Figure 3.18 (b)) and SSA (Figure 3.18 (c)) are not efficient for erratic noise attenuation. Figure 3.19 show the error panels of the three methods. Still, we can find that robust SSA preserves signal

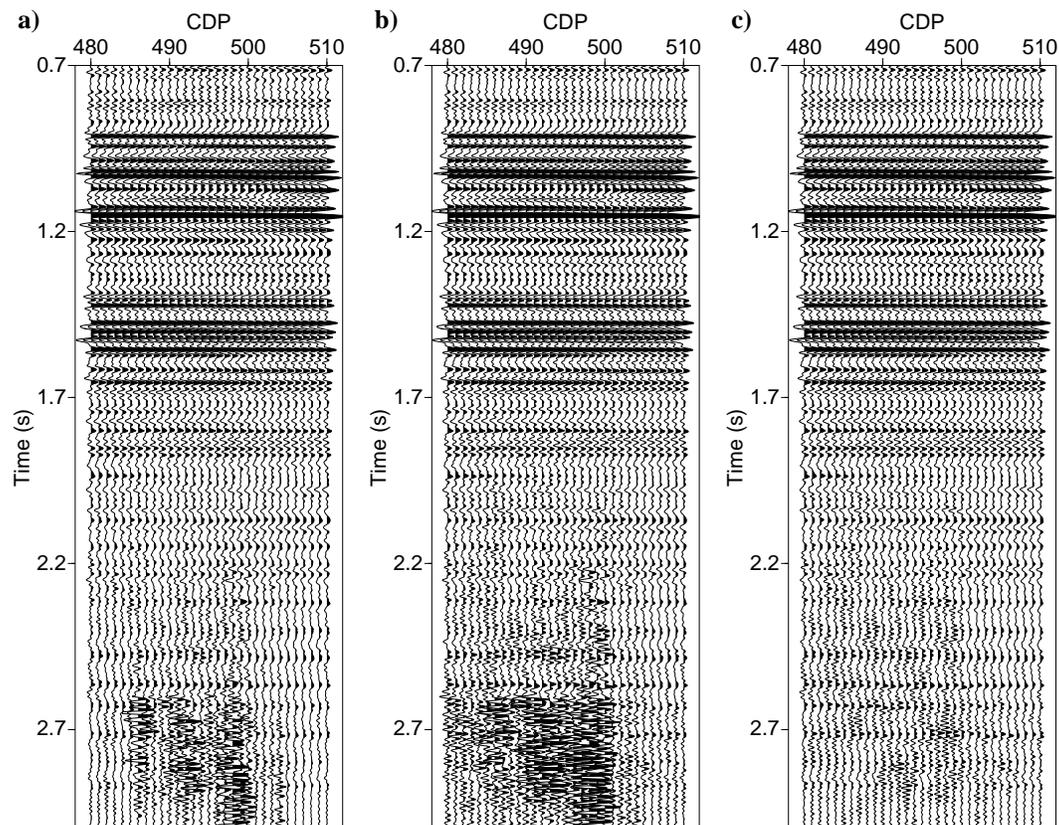


Figure 3.14: The comparison of results of the data in the left rectangular window by three different methods. (a) Data after f - x deconvolution filtering. (b) Data after classical SSA filtering. (c) Data after robust SSA filtering.

f - x deconvolution do not perform well. The field data examples from Western Canadian Sedimentary Basin and Alaska are used to analyze the performance of the new algorithm on real data. One possible concern is the computation cost of the robust algorithm. Computational time can be reduced by adopting windowing strategies to minimize the size of the Hankel matrices to factorize. Another strategy is to truncate the number of iterations of the alternating minimization algorithm and IRLS solvers in a way that an inexact factorization is estimated. We have noticed that an inexact factorization can yield better results than conventional non-robust Rank-reduction via the truncated SVD.

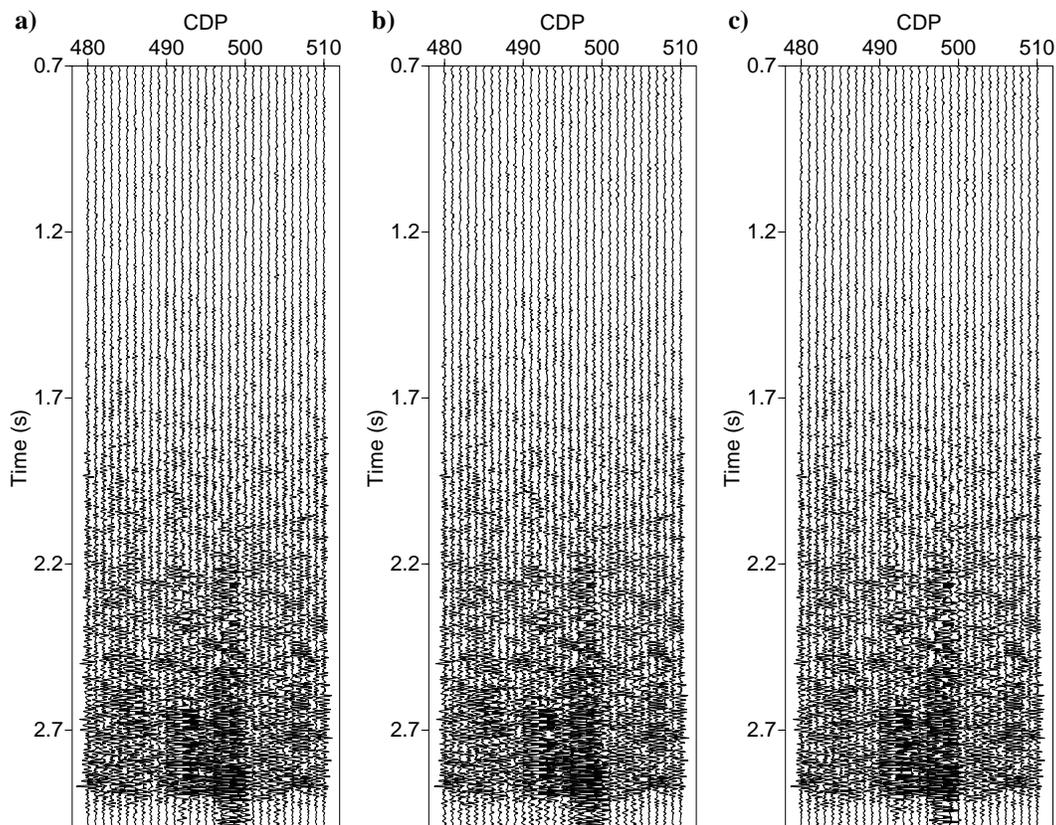


Figure 3.15: The comparison of error panels of three different methods in the left rectangular window. Error panels of f - x deconvolution (a), SSA (b), and robust SSA (c).

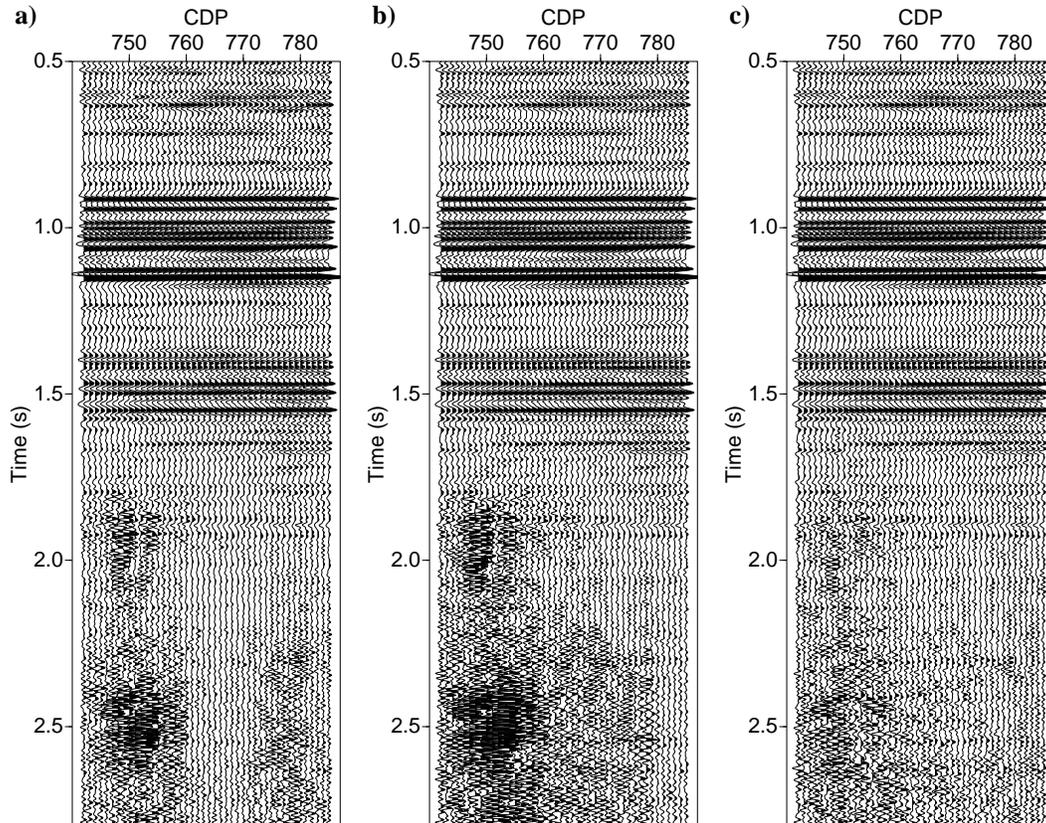
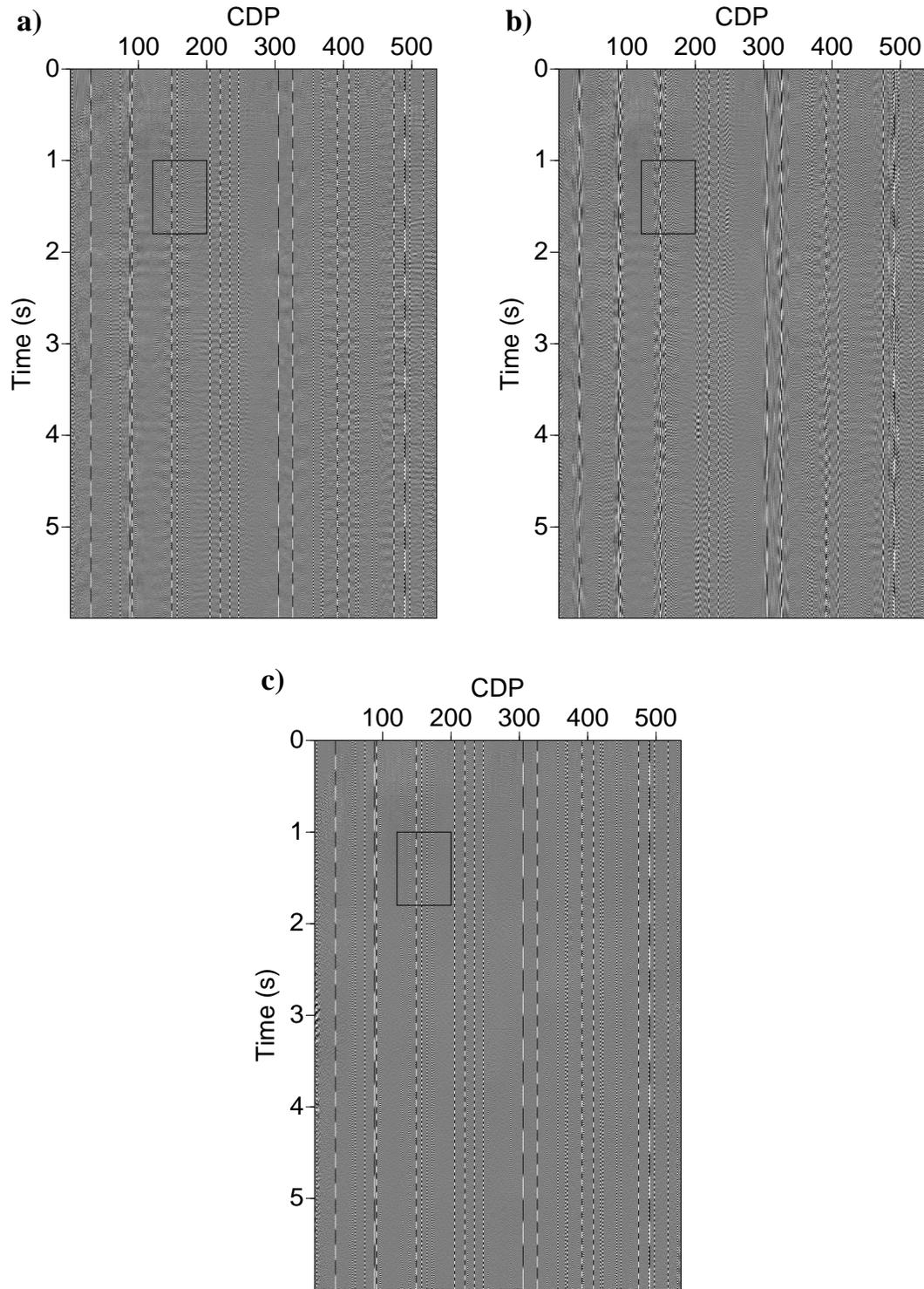


Figure 3.16: The comparison of results of the data in the right rectangular window by three different methods. (a) Data after $f-x$ deconvolution filtering. (b) Data after classical SSA filtering. (c) Data after robust SSA filtering.

Figure 3.19: Error panels of (a) $f-x$ deconvolution, (b) SSA, (c) robust SSA.

CHAPTER 4

Matrix rank reduction approximated by nuclear-norm minimization

4.1 Introduction

As mentioned in the introduction, seismic data acquired in field may have too large spatial sampling interval, may have large gap between traces, or may be irregularly sampled in space. Cadzow/SSA based methods have been applied for irregularly decimated seismic data reconstruction (Trickett et al., 2010; Oropeza and Sacchi, 2011; Gao et al., 2013). In this case, the constructed Hankel matrix is not only perturbed by random Gaussian noise but also incomplete. Many elements of the matrix are missing in an irregular pattern. Trickett et al. (2010) proposed a Cadzow filtering based method for multidimensional trace interpolation. It applies an algorithm of matrix completion instead of the direct TSVD on the incomplete Hankel matrix. Oropeza and Sacchi (2011) proposed a seismic data reconstruction method similar with the projection onto convex sets (POCS) (Abma and Kabir, 2006) that replaces the frequency spectrum thresholding in POCS by MSSA filtering. The rank reduction is based on a randomized SVD instead of naive SVD for acceleration. Gao et al. (2013) extended the MSGEO-2013-0350SA reconstruction to 5D. The rank reduction is based on Lanczos bidiagonalization, and the Toeplitz matrix-vector multiplication is accelerated by the Fast Fourier Transform (FFT). These methods works for regular data grid with irregular missing pattern. They can not deal with aliasing problem. Naghizadeh and Sacchi (2013) proposed a MSSA/Cadzow based reconstruction algorithm for interpolating *regularly* sampled seismic data. It extract information from low frequencies to recover the regularly missing information at high frequencies.

The methods mentioned above do not consider erratic data (Claerbout and Muir, 1973).

the entries $\{\tilde{\mathbf{D}}_i, i \in \Gamma\}$ are recorded. Then, the \mathcal{P}_Γ indicates the projection onto the space of vectors supported on Γ . We call it the sampling operator, $\mathbf{D} = \mathcal{P}_\Gamma(\tilde{\mathbf{D}})$. Most of the singular spectrum analysis methods apply least-squares minimization in the rank reduction, e.g. the truncated SVD (Trickett, 2008), the method based on Random SVD (Oropeza and Sacchi, 2011) and the method based on Lanczos bidiagonalization (Gao et al., 2013). It is well known that the least-squares process is not robust. Even one single outlier will result in an erroneous solution. The erratic noise in the seismic data need robust algorithm to suppress. The extraction of low-rank component from the incomplete and corrupted matrix is achieved by solving a low-rank matrix recovery problem (Candès et al., 2009).

4.2.3 Low-rank matrix recovery

We utilize a robust low rank approximation other than the truncated SVD to recover the low-rank component from the partly observed and grossly corrupted matrix \mathbf{M} . Our Robust SSA algorithm is summarized as follows

$$\begin{aligned} \text{For each frequency slice :} \\ \hat{\mathbf{D}} = \mathcal{A}(\mathcal{M}_\mathcal{R}(\mathcal{H}(\mathbf{D}))), \end{aligned} \quad (4.1)$$

where $\mathcal{M}_\mathcal{R}$ denotes the operator for solving the low-rank matrix recovery problem, $\hat{\mathbf{D}}$ is the reconstructed frequency slice. Let $\tilde{\mathbf{M}}$ denotes the Hankel matrix from the completely sampled data $\tilde{\mathbf{D}}$, i.e. $\tilde{\mathbf{M}} = \mathcal{H}(\tilde{\mathbf{D}})$. \mathcal{H} is a Hankel operator. Matrix $\tilde{\mathbf{M}}$ can be decomposed to three components as:

$$\tilde{\mathbf{M}} = \mathbf{L} + \mathbf{S} + \mathbf{N}, \quad (4.2)$$

where \mathbf{L} is the low rank matrix embedded from the f - x signal, \mathbf{S} is a sparse matrix corresponding to impulsive noise and \mathbf{N} is a dense perturbation matrix representing Gaussian noise. If there is only impulsive noise ($\mathbf{N} = \mathbf{0}$), the problem is recovering low-rank component from completely observed but impulsive noise corrupted matrix. It is also referred to as the robust principal component analysis problem (Candès et al., 2009). The solution can be obtained from solving the matrix rank minimization problem

$$\begin{aligned} \min_{\mathbf{L}, \mathbf{S}} \text{rank}(\mathbf{L}) + \gamma \|\mathbf{S}\|_0, \\ \text{subject to } \tilde{\mathbf{M}} = \mathbf{L} + \mathbf{S}, \end{aligned} \quad (4.3)$$

where γ is a trade-off parameter balancing the low-rank of \mathbf{L} and the sparsity of \mathbf{S} . Unfortunately, both rank function and ℓ_0 function are non-convex. This low-rank matrix recovery problem is NP-hard because the combinational nature of rank function and ℓ_0 norm. Candès et al. (2009) proved that the low-rank and sparse component can be solved by a relaxed

convex program, the Principal Component Pursuit

$$\begin{aligned} \min_{\mathbf{L}, \mathbf{S}} \quad & \|\mathbf{L}\|_* + \lambda \|\mathbf{S}\|_1, \\ \text{subject to} \quad & \tilde{\mathbf{M}} = \mathbf{L} + \mathbf{S}, \end{aligned} \quad (4.4)$$

the rank minimization is relaxed to the nuclear norm minimization and the ℓ_0 norm minimization is relaxed to ℓ_1 norm minimization, λ is a trade-off parameter to balance the sparsity and low rank. The nuclear-norm guarantees the low rank of component \mathbf{L} , the ℓ_1 norm induces the sparsity of component \mathbf{S} , i.e. the robustness of this recovery algorithm with respect to outliers. However, the seismic data are usually corrupted with dense Gaussian noise, i.e. $\mathbf{N} \neq \mathbf{0}$. The problem changes to the recovery of low-rank matrix from a matrix that is corrupted with sparse impulsive noise and small dense Gaussian noise. Zhou et al. (2010) proved that this problem can be solved by the convex program Stable Principal Component Pursuit

$$\begin{aligned} \min_{\mathbf{L}, \mathbf{S}} \quad & \|\mathbf{L}\|_* + \lambda \|\mathbf{S}\|_1, \\ \text{subject to} \quad & \|\tilde{\mathbf{M}} - \mathbf{L} - \mathbf{S}\|_F \leq \delta, \end{aligned} \quad (4.5)$$

where the Frobenius norm induce the stability towards Gaussian noise perturbation, δ is the Gaussian noise level.

When the observed data is under sampled ($\mathbf{D} = \mathcal{P}_\Gamma(\tilde{\mathbf{D}})$), the constructed Hankel matrix has missing elements. Suppose that Ω is the support of nonzero elements of matrix \mathbf{M} , i.e. entries $\{\tilde{\mathbf{M}}_{ij}, (i, j) \in \Omega\}$ are the recorded elements. \mathcal{P}_Ω denotes the sampling operator acted on the complete observed matrix $\tilde{\mathbf{M}}$, i.e. $\mathbf{M} = \mathcal{P}_\Omega(\tilde{\mathbf{M}})$. Now, the problem changes to recover the low-rank component from a fraction of the grossly corrupted and randomly perturbed entries of the matrix. It can be expressed as

$$\begin{aligned} \min_{\mathbf{L}, \mathbf{S}} \quad & \|\mathbf{L}\|_* + \lambda \|\mathbf{S}\|_1, \\ \text{subject to} \quad & \|\mathcal{P}_\Omega(\tilde{\mathbf{M}} - \mathbf{L} - \mathbf{S})\|_F \leq \delta. \end{aligned} \quad (4.6)$$

When \mathcal{P}_Ω is the identity operator, 4.6 recovers low-rank matrix from completely observed, Gaussian and impulsive noise corrupted matrix 4.5. When \mathcal{P}_Ω is the identity operator and $\sigma = 0$, it recovers low-rank matrix from completely observed, impulsive noise corrupted matrix 4.4. When $\sigma = 0$, $\lambda = 0$ and $\mathbf{S} = \mathbf{0}$, it solves the matrix completion problem (Candès and Recht, 2009). When $\lambda = 0$ and $\mathbf{S} = \mathbf{0}$, it solves the matrix completion with Gaussian noise problem (Candès and Plan, 2009).

The penalized version of convex program 4.6 is

$$\min_{\mathbf{L}, \mathbf{S}} \quad \|\mathbf{L}\|_* + \lambda \|\mathbf{S}\|_1 + \frac{1}{2\mu} \|\mathcal{P}_\Omega(\tilde{\mathbf{M}} - \mathbf{L} - \mathbf{S})\|_F^2, \quad (4.7)$$

Equation 4.7 is modified as

$$\begin{aligned} \min_{\mathbf{L}, \mathbf{S}, \mathbf{Z}} \quad & \|\mathbf{L}\|_* + \lambda \|\mathbf{S}\|_1 + \frac{1}{2\mu} \|\mathcal{P}_\Omega(\mathbf{Z})\|_F^2, \\ \text{subject to} \quad & \mathbf{L} + \mathbf{S} + \mathbf{Z} = \mathbf{M}. \end{aligned} \quad (4.10)$$

The elements outside the set Ω in $\mathbf{L} + \mathbf{S}$ are compensated by corresponding elements in \mathbf{Z} . Then the augmented Lagrangian function of Problem 4.10 is

$$\mathcal{L}_A(\mathbf{L}, \mathbf{S}, \mathbf{Z}, \mathbf{Y}, \beta) = \|\mathbf{L}\|_* + \lambda \|\mathbf{S}\|_1 + \frac{1}{2\mu} \|\mathcal{P}_\Omega(\mathbf{Z})\|_F^2 - \langle \mathbf{Y}, \mathbf{L} + \mathbf{S} + \mathbf{Z} - \mathbf{M} \rangle + \frac{\beta}{2} \|\mathbf{L} + \mathbf{S} + \mathbf{Z} - \mathbf{M}\|_F^2, \quad (4.11)$$

where \mathbf{Y} is the Lagrange multiplier, β is the penalty parameter. The general augmented Lagrangian method optimizes all the variables together $(\mathbf{L}^{k+1}, \mathbf{S}^{k+1}, \mathbf{Z}^{k+1})$ at step 3 in Algorithm 2 and then update the Lagrange Multiplier \mathbf{Y}^{k+1} and penalize parameter β^{k+1} . Tao and Yuan (2011) further explore the separable structure of the cost function and constraint in 4.11 and propose a more efficient alternating splitting augmented Lagrangian method (ASALM), which compute the three components separately, i.e. \mathbf{L}^{k+1} , \mathbf{S}^{k+1} and then \mathbf{Z}^{k+1} . The idea of splitting is similar with the inexact augmented Lagrangian method (Lin et al., 2010) and the alternating direction method (ADM) (Yuan and Yang, 2009). The three variables are updated via solving three sub-problems

$$\begin{aligned} \mathbf{Z}^{k+1} &:= \arg \min_{\mathbf{Z}} \frac{1}{2\mu} \|\mathcal{P}_\Omega(\mathbf{Z})\|_F^2 - \langle \mathbf{Y}^k, \mathbf{L}^k + \mathbf{S}^k + \mathbf{Z} - \mathbf{M} \rangle + \frac{\beta}{2} \|\mathbf{L}^k + \mathbf{S}^k + \mathbf{Z} - \mathbf{M}\|_F^2, \\ \mathbf{S}^{k+1} &:= \arg \min_{\mathbf{S}} \lambda \|\mathbf{S}\|_1 - \langle \mathbf{Y}^k, \mathbf{L}^k + \mathbf{S} + \mathbf{Z}^{k+1} - \mathbf{M} \rangle + \frac{\beta}{2} \|\mathbf{L}^k + \mathbf{S} + \mathbf{Z}^{k+1} - \mathbf{M}\|_F^2, \\ \mathbf{L}^{k+1} &:= \arg \min_{\mathbf{L}} \|\mathbf{L}\|_* - \langle \mathbf{Y}^k, \mathbf{L} + \mathbf{S}^{k+1} + \mathbf{Z}^{k+1} - \mathbf{M} \rangle + \frac{\beta}{2} \|\mathbf{L} + \mathbf{S}^{k+1} + \mathbf{Z}^{k+1} - \mathbf{M}\|_F^2, \\ \mathbf{Y}^{k+1} &:= \mathbf{Y}^k - \beta(\mathbf{L}^{k+1} + \mathbf{S}^{k+1} + \mathbf{Z}^{k+1} - \mathbf{M}), \end{aligned} \quad (4.12)$$

where the penalize parameter β is fixed in the ASALM method. The most important benefit is that each subproblem has closed form solution. They can be obtained by setting the gradient (Frobenius norm) or subgradient (ℓ_1 norm, nuclear-norm) to zero. It's easy to see that the update in Equation 4.12 is the same as the following problems (Tao and Yuan, 2011)

$$\begin{aligned} \mathbf{Z}^{k+1} &:= \arg \min_{\mathbf{Z}} \frac{1}{2\mu} \|\mathcal{P}_\Omega(\mathbf{Z})\|_F^2 + \frac{\beta}{2} \|\mathbf{L}^k + \mathbf{S}^k + \mathbf{Z} - \frac{1}{\beta} \mathbf{Y}^k - \mathbf{M}\|_F^2, \\ \mathbf{S}^{k+1} &:= \arg \min_{\mathbf{S}} \lambda \|\mathbf{S}\|_1 + \frac{\beta}{2} \|\mathbf{L}^k + \mathbf{S} + \mathbf{Z}^{k+1} - \frac{1}{\beta} \mathbf{Y}^k - \mathbf{M}\|_F^2, \\ \mathbf{L}^{k+1} &:= \arg \min_{\mathbf{L}} \|\mathbf{L}\|_* + \frac{\beta}{2} \|\mathbf{L} + \mathbf{S}^{k+1} + \mathbf{Z}^{k+1} - \frac{1}{\beta} \mathbf{Y}^k - \mathbf{M}\|_F^2, \\ \mathbf{Y}^{k+1} &:= \mathbf{Y}^k - \beta(\mathbf{L}^{k+1} + \mathbf{S}^{k+1} + \mathbf{Z}^{k+1} - \mathbf{M}), \end{aligned} \quad (4.13)$$

where the update of \mathbf{S}^{k+1} and \mathbf{L}^{k+1} can be obtained from two well-known *shrinkage operators*.

Usually, the soft shrinkage operator (Chen et al., 1998) $\mathcal{S}_\tau : \mathbb{R} \rightarrow \mathbb{R}$ is defined as $\mathcal{S}_\tau(x) = \text{sgn}(x)\max(|x| - \tau, 0)$. Because we apply the method in frequency domain, we use the soft shrinkage operator defined in the complex domain (Sardy, 2000): $\mathcal{S}_\tau : \mathbb{C} \rightarrow \mathbb{C}$ is defined as $\mathcal{S}_\tau(x) = \frac{x}{|x|}\max(|x| - \tau, 0)$. It is extended to the case of matrices

$$(\mathcal{S}_\tau(\mathbf{X}))_{ij} := \frac{\mathbf{X}_{ij}}{|\mathbf{X}_{ij}|} \max(|\mathbf{X}_{ij}| - \tau, 0), \quad \mathbf{X} \in \mathbb{C}^{m \times n}. \quad (4.14)$$

$\mathcal{S}_\tau(\mathbf{X})$ is the solution of the following minimization problem

$$\min_{\mathbf{Y}} \tau \|\mathbf{Y}\|_1 + \frac{1}{2} \|\mathbf{Y} - \mathbf{X}\|_F^2. \quad (4.15)$$

Suppose the rank r matrix $\mathbf{X} \in \mathbb{C}^{m \times n}$ has the following singular value decomposition

$$\mathbf{X} = \mathbf{U}\mathbf{\Sigma}\mathbf{V}^H, \quad (4.16)$$

where $\mathbf{U} \in \mathbb{C}^{m \times r}$ is the matrix containing left singular vectors, $\mathbf{V} \in \mathbb{C}^{n \times r}$ is the matrix containing right singular vectors and $\mathbf{\Sigma} = \text{diag}\{\sigma_1, \sigma_2, \dots, \sigma_r\}$ is the matrix containing singular values. The singular value shrinkage operator \mathcal{D}_τ applied on \mathbf{X} is defined as following (Cai et al., 2008)

$$\mathcal{D}_\tau(\mathbf{X}) = \mathbf{U}\mathcal{S}_\tau(\mathbf{\Sigma})\mathbf{V}^H. \quad (4.17)$$

$\mathcal{D}_\tau(\mathbf{X})$ is the solution of the following minimization problem

$$\min_{\mathbf{Y}} \tau \|\mathbf{Y}\|_* + \frac{1}{2} \|\mathbf{Y} - \mathbf{X}\|_F^2. \quad (4.18)$$

So the solutions of Equation 4.13 can be expressed using the above shrinkage operator and singular value shrinkage operator. The alternating splitting augmented Lagrangian method (ASALM) (Tao and Yuan, 2011) is summarized as following Algorithm 3

The proof of convergence of the ASALM algorithm is given in Tao and Yuan (2011). The dominant cost of the algorithm is given by the cost of the singular value shrinkage operator.

4.2.5 Parameter Selection and Stopping Criterion

Candès et al. (2009) and Zhou et al. (2010) proved that the selection of $\lambda = 1/\sqrt{\max(m, n)}$ can guarantee good recovery result in the (Stable) Principal Component Pursuit program. It is fixed in the algorithm. μ and β are tuning parameters that depend on the data. Tao

Algorithm 3 Alternating Splitting Augmented Lagrangian Method (ASALM) for Low Rank Matrix Recovery

- 1: **Initialization:** $\mathbf{L}^0 = \mathbf{0}, \mathbf{S}^0 = \mathbf{0}, \mathbf{Y}^0 = \mathbf{0}, \lambda = 1/\sqrt{\max(m, n)}, \mu, \beta.$
- 2: **while** not converge **do**
- 3: Compute $\mathbf{T}^k = \frac{1}{\beta}\mathbf{Y}^k + \mathbf{M} - \mathbf{L}^k - \mathbf{S}^k.$
- 4: Compute $\mathbf{Z}^{k+1}:$

$$\mathbf{Z}_{ij}^{k+1} = \begin{cases} \mathbf{T}_{ij}^k & \text{when } (i, j) \notin \Omega; \\ \frac{\mu\beta}{1 + \mu\beta}\mathbf{T}_{ij}^k & \text{when } (i, j) \in \Omega. \end{cases}$$

- 5: Compute \mathbf{S}^{k+1} : $\mathbf{S}^{k+1} = \mathcal{S}_{\lambda/\beta}(\frac{1}{\beta}\mathbf{Y}^k + \mathbf{M} - \mathbf{L}^k - \mathbf{Z}^{k+1}).$
 - 6: Compute \mathbf{L}^{k+1} : $\mathbf{L}^{k+1} = \mathcal{D}_{1/\beta}(\frac{1}{\beta}\mathbf{Y}^k + \mathbf{M} - \mathbf{S}^{k+1} - \mathbf{Z}^{k+1}).$
 - 7: Update \mathbf{Y}^{k+1} : $\mathbf{Y}^{k+1} = \mathbf{Y}^k + \beta(\mathbf{M} - \mathbf{L}^{k+1} - \mathbf{S}^{k+1} - \mathbf{Z}^{k+1}).$
 - 8: **end while**
-

and Yuan (2011) recommend to choose the parameters based on the following strategy

$$\begin{aligned} \mu &= \frac{1}{10}\sqrt{\min(m, n) + \sqrt{8\min(m, n)\sigma}}, \\ \beta &= \eta\frac{|\Omega|}{\|\mathbf{M}\|_1}, \end{aligned} \tag{4.19}$$

where σ is the standard derivation (SD) of Gaussian noise. The coefficient η depends on the percentage of the outliers in the matrix, $|\Omega|$ is the cardinality of the set Ω , i.e. the number of elements of set Ω . The stopping criterion is chosen to be (Tao and Yuan, 2011)

$$SP = \frac{\|(\mathbf{L}^{k+1}, \mathbf{S}^{k+1}) - (\mathbf{L}^k, \mathbf{S}^k)\|_F}{\|(\mathbf{L}^k, \mathbf{S}^k)\|_F + 1} \leq \xi\sigma, \tag{4.20}$$

where ξ is a coefficient which is tunable. The stopping criterion measures the change of the low-rank component and sparse component in two consecutive iterations.

4.3 Examples

We present two synthetic examples to test the proposed algorithm.

4.3.1 Synthetic Example 1

We first test a simple synthetic data that is incomplete and corrupted with large amplitude erratic noise (coherent in temporal direction). Because the outliers do not appear in all the frequencies, we analyze the behavior of the Algorithm 3 in different situations. For

the frequency slices which contain outliers and missing elements, it is actually a Gaussian noiseless ($\mathbf{N} = \mathbf{0}$) low-rank matrix recovery problem ($\sigma = 0$ in convex program 4.6).

$$\begin{aligned} & \min_{\mathbf{L}, \mathbf{S}} \|\mathbf{L}\|_* + \lambda \|\mathbf{S}\|_1, \\ & \text{subject to } \mathcal{P}_\Omega(\mathbf{L} + \mathbf{S}) = \mathcal{P}_\Omega(\tilde{\mathbf{M}}) = \mathbf{M}. \end{aligned} \quad (4.21)$$

Similarly, with the replacement $\mathbf{L} + \mathbf{S} + \mathbf{Z} = \mathbf{M}$, it can be changed to

$$\begin{aligned} & \min_{\mathbf{L}, \mathbf{S}} \|\mathbf{L}\|_* + \lambda \|\mathbf{S}\|_1, \\ & \text{subject to } \mathbf{L} + \mathbf{S} + \mathbf{Z} = \mathbf{M}, \mathcal{P}_\Omega(\mathbf{Z}) = \mathbf{0}, \end{aligned} \quad (4.22)$$

In this case, the augmented Lagrangian is

$$\mathcal{L}_\mathcal{A}(\mathbf{L}, \mathbf{S}, \mathbf{Z}, \mathbf{Y}, \beta) = \|\mathbf{L}\|_* + \lambda \|\mathbf{S}\|_1 - \langle \mathbf{Y}, \mathbf{L} + \mathbf{S} + \mathbf{Z} - \mathbf{M} \rangle + \frac{\beta}{2} \|\mathbf{L} + \mathbf{S} + \mathbf{Z} - \mathbf{M}\|_F^2, \quad (4.23)$$

with $\mathcal{P}_\Omega(\mathbf{Z}) = 0$. The algorithm for convex program 4.21 is a special case of Algorithm 3 with parameter $\mu = 0$.

For the frequency slices which do not contain outliers, they only contain missing elements. The constructed Hankel matrix is incomplete but noise free. The problem changes to a noiseless matrix completion problem

$$\begin{aligned} & \min_{\mathbf{L}} \|\mathbf{L}\|_*, \\ & \text{subject to } \mathcal{P}_\Omega(\mathbf{L}) = \mathcal{P}_\Omega(\tilde{\mathbf{M}}) = \mathbf{M}. \end{aligned} \quad (4.24)$$

with the replacement $\mathbf{L} + \mathbf{Z} = \mathbf{M}$, it is changed to

$$\begin{aligned} & \min_{\mathbf{L}} \|\mathbf{L}\|_*, \\ & \text{s.t. } \mathbf{L} + \mathbf{Z} = \mathbf{M}, \mathcal{P}_\Omega(\mathbf{Z}) = \mathbf{0}. \end{aligned} \quad (4.25)$$

The augmented Lagrangian is

$$\mathcal{L}_\mathcal{A}(\mathbf{L}, \mathbf{Z}, \mathbf{Y}, \beta) = \|\mathbf{L}\|_* - \langle \mathbf{Y}, \mathbf{L} + \mathbf{Z} - \mathbf{M} \rangle + \frac{\beta}{2} \|\mathbf{L} + \mathbf{Z} - \mathbf{M}\|_F^2, \quad (4.26)$$

with $\mathcal{P}_\Omega(\mathbf{Z}) = 0$. The algorithm for noiseless matrix completion problem is (Lin et al., 2010)

Algorithm 4 is a particular case of Algorithm 3 with $\mu = 0$ and $\mathbf{S} = \mathbf{0}$. With a good thresholding parameter λ/β in Algorithm 3, the elements in \mathbf{S} does not contain the signal. That is to say, the matrix \mathbf{S} will stay as zero matrix during the iterations. Then, it is

Algorithm 4 Alternating Splitting Augmented Lagrangian Method (ASALM) for Matrix Completion

- 1: **Initialization:** $\mathbf{L}^0 = \mathbf{0}, \mathbf{Y}^0 = \mathbf{0}, \beta$.
- 2: **while** not converge **do**
- 3: Compute $\mathbf{T}^k = \frac{1}{\beta} \mathbf{Y}^k + \mathbf{M} - \mathbf{L}^k$.
- 4: Compute \mathbf{Z}^{k+1} :

$$\mathbf{z}_{ij}^{k+1} = \begin{cases} \mathbf{T}_{ij}^k & \text{when } (i, j) \notin \Omega; \\ 0 & \text{when } (i, j) \in \Omega. \end{cases}$$

- 5: Compute \mathbf{L}^{k+1} : $\mathbf{L}^{k+1} = \mathcal{D}_{1/\beta}(\frac{1}{\beta} \mathbf{Y}^k + \mathbf{M} - \mathbf{Z}^{k+1})$.
 - 6: Update \mathbf{Y}^{k+1} : $\mathbf{Y}^{k+1} = \mathbf{Y}^k + \beta(\mathbf{M} - \mathbf{L}^{k+1} - \mathbf{Z}^{k+1})$.
 - 7: **end while**
-

reasonable to use Algorithm 3 with setting $\mu = 0$ for all the frequency slices in this synthetic example.

The synthetic data has 80 traces with time sampling interval 0.004 s. There are 5 traces corrupted with large amplitude (1 to 7 times the amplitude of wavelet) time coherent noise and 50% traces randomly missing. Figure 4.1 (d) shows the noise free data, Figure 4.1 (a) shows the data with missing traces and corrupted with erratic noise. We use Algorithm 3 to recover the low-rank component \mathbf{L} and then the reconstructed data $\hat{\mathbf{D}}$. The frequency band to be processed is 1-40 Hz. For parameter selection, we simply set $\mu = 0$ and $\beta = 0.15 \frac{|\Omega|}{\|\mathbf{M}\|_1}$. The stopping criterion is chosen as: $SP \leq 10^{-7}$. Figure 4.1 (b) is the reconstructed result, Figure 4.1 (e) is the difference between noise free data and the reconstructed data. Figure 4.1 (c) is the recovered sparse component. We can see that the robust SSA via low-rank matrix recovering exactly reconstructed the signal and also the time coherent noise. We use the quality factor $Q = 10 \log \frac{\|d^0\|_F^2}{\|d^0 - \hat{d}\|_F^2}$ to evaluate the result. The $Q = 114$ in this synthetic example.

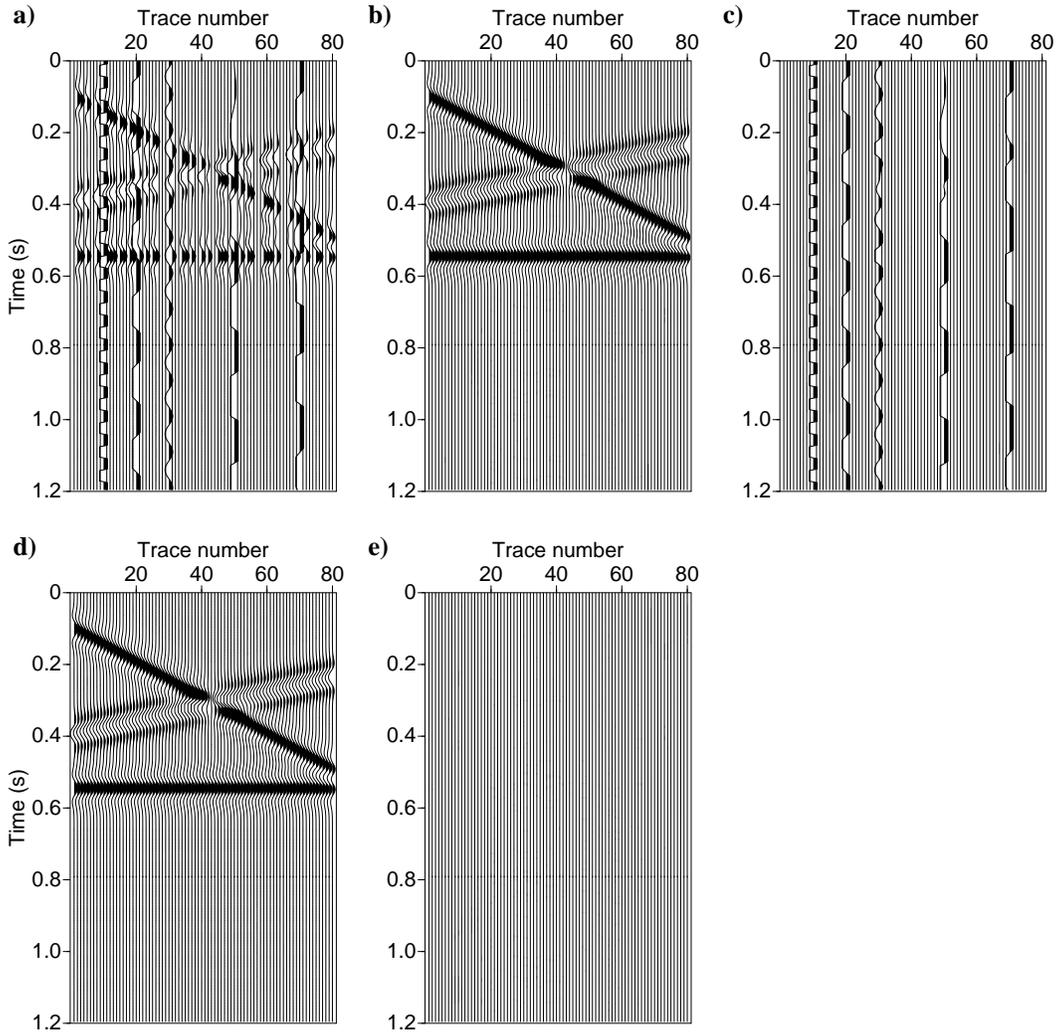


Figure 4.1: (a) Synthetic seismic data with 50% traces missing and 5 traces corrupted with erratic noise. (b) Data filtered by robust SSA via low-rank matrix recovering. (c) Sparse erratic noise obtained from robust SSA. (d) Noise-free synthetic data. (e) Difference section between noise-free synthetic data and data filtered by robust SSA.

4.3.2 Synthetic Example 2

The synthetic data is both undersampled and corrupted with large amplitude time coherent noise and smoothed Gaussian noise. If frequency slice \mathbf{D} has outliers, the recovering of \mathbf{L} is achieved by solving convex program 4.6.

If there is no outlier in frequency slice \mathbf{D} , it changes to a Gaussian-noisy matrix completion problem

$$\begin{aligned} \min_{\mathbf{L}, \mathbf{Z}} \quad & \|\mathbf{L}\|_* + \frac{1}{2\mu} \|\mathcal{P}_\Omega(\mathbf{Z})\|_F^2, \\ \text{subject to} \quad & \mathbf{L} + \mathbf{Z} = \mathbf{M}. \end{aligned} \quad (4.27)$$

The augmented Lagrangian function is

$$\mathcal{L}_{\mathcal{A}}(\mathbf{L}, \mathbf{Z}, \mathbf{Y}, \beta) = \|\mathbf{L}\|_* + \frac{1}{2\mu} \|\mathcal{P}_\Omega(\mathbf{Z})\|_F^2 - \langle \mathbf{Y}, \mathbf{L} + \mathbf{Z} - \mathbf{M} \rangle + \frac{\beta}{2} \|\mathbf{L} + \mathbf{Z} - \mathbf{M}\|_F^2 \quad (4.28)$$

The algorithm of alternating splitting augmented Lagrangian method for Gaussian-noisy matrix completion problem is

Algorithm 5 Alternating Splitting Augmented Lagrangian Method (ASALM) for Matrix Completion with Noise

- 1: **Initialization:** $\mathbf{L}^0 = \mathbf{0}$, $\mathbf{Y}^0 = \mathbf{0}$, μ , β .
- 2: **while** not converge **do**
- 3: Compute $\mathbf{T}^k = \frac{1}{\beta} \mathbf{Y}^k + \mathbf{M} - \mathbf{L}^k$.
- 4: Compute \mathbf{Z}^{k+1} :

$$\mathbf{Z}_{ij}^{k+1} = \begin{cases} \mathbf{T}_{ij}^k & \text{when } (i, j) \notin \Omega; \\ \frac{\mu\beta}{1 + \mu\beta} \mathbf{T}_{ij}^k & \text{when } (i, j) \in \Omega. \end{cases}$$

- 5: Compute \mathbf{L}^{k+1} : $\mathbf{L}^{k+1} = \mathcal{D}_{1/\beta}(\frac{1}{\beta} \mathbf{Y}^k + \mathbf{M} - \mathbf{Z}^{k+1})$.
 - 6: Update \mathbf{Y}^{k+1} : $\mathbf{Y}^{k+1} = \mathbf{Y}^k + \beta(\mathbf{M} - \mathbf{L}^{k+1} - \mathbf{Z}^{k+1})$.
 - 7: **end while**
-

Algorithm 5 is a special case of Algorithm 3 with $\mathbf{S} = \mathbf{0}$. In this situation, if a suitable threshold parameter λ/β is selected in Algorithm 3, matrix \mathbf{S} will remain a zero matrix. Algorithm 3 can be applied on all the frequency slices. Figure 4.2 (d) is the noise-free data, Figure 4.2 (a) is the incomplete and corrupted data. The erratic noise added is the same with the one in Example 1. There are 25% traces missing in the original data set. The SNR of the Gaussian noise is 2. The frequency band to be processed is 1-40 Hz like previous examples. As to the parameters, $\mu = 0.1 \sqrt{\min(m, n) + \sqrt{8\min(m, n)}}\sigma$, $\beta = 0.1 \frac{|\Omega|}{\|\mathbf{M}\|_1}$. The stopping criterion is selected to be $SP \leq 10^{-7}\sigma$. Figure 4.2 (b) is the reconstructed result. We can find that the algorithm removed the Gaussian noise and erratic noise and also recovered the missing traces. The quality factor of the reconstructed result is $Q = 24$. Figure 4.2 (c) shows the erratic noise recovered by the sparse matrix \mathbf{S} . However, there is a little energy in the difference section Figure 4.2 (e).

4.4 Summary

In this chapter, we propose a robust SSA method for erratic noise suppression and missing data interpolation via solving low-rank matrix recovery problem. The low-rank matrix recovery is achieved by solving a convex program, i.e. minimizing the weighted combination of nuclear-norm ℓ_1 norm and Frobenius norm. We present some preliminary synthetic results. It shows that the proposed algorithm can remove Gaussian and erratic noise and interpolating missing traces simultaneously. There are several possible directions for the future works. First, the soft thresholding of the singular values allows the processing of curvature events situation. It is natural to extend the method to 3D and 5D situations.

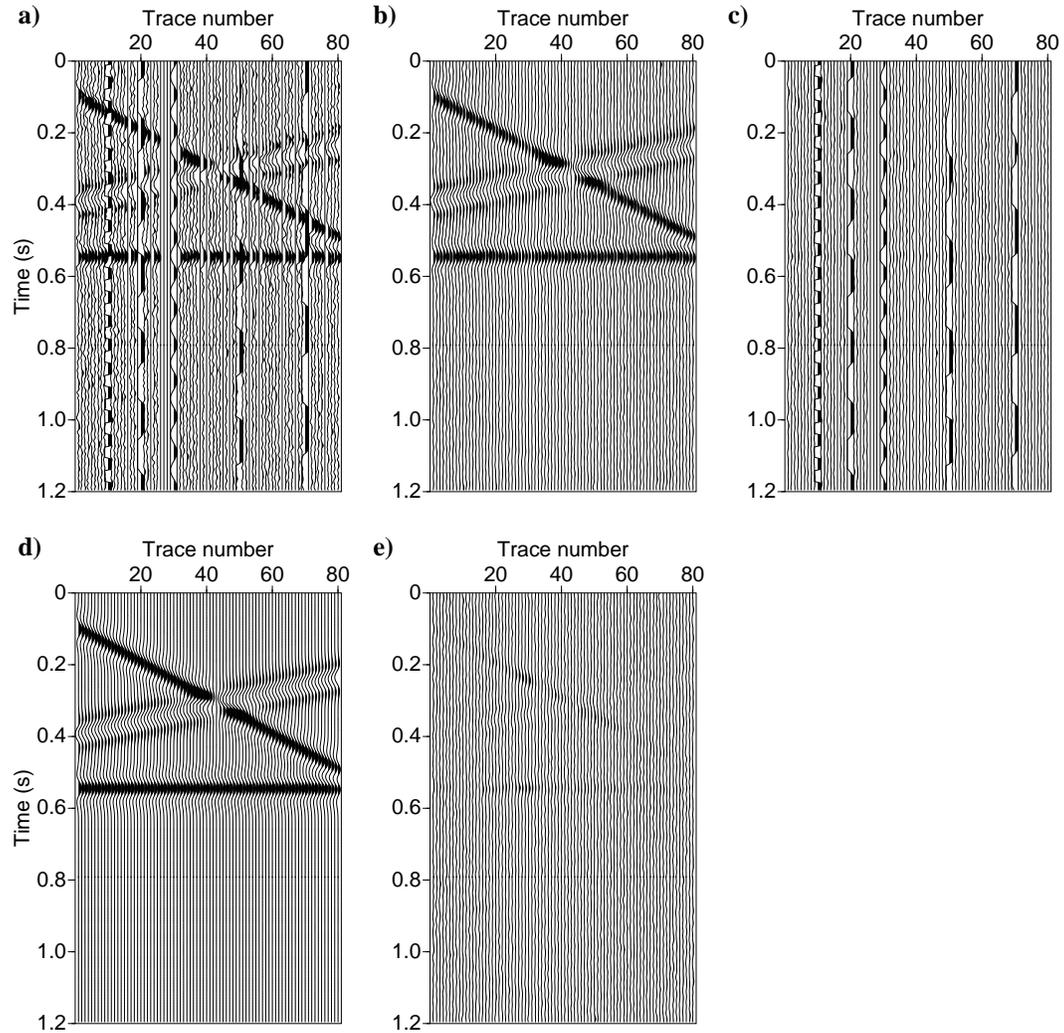


Figure 4.2: (a) Synthetic seismic data with 25% traces missing, Gaussian noise (SNR=2) and 5 traces corrupted with erratic noise. (b) Data filtered by robust SSA via low-rank matrix recovering. (c) Sparse erratic noise obtained from robust SSA. (d) Noise-free synthetic data. (e) Difference section between noise-free synthetic data and data filtered by robust SSA.

CHAPTER 5

Conclusions

This thesis focuses on the subject of non-Gaussian seismic noise suppression in seismic data processing. More specially, we propose robust matrix rank-reduction methods for simultaneous Gaussian and non-Gaussian seismic noise attenuation.

I have proposed a new method that permits to robustify the SSA denoising method. This is achieved by introducing robust matrix factorization and nuclear norm minimization into the formulation of the SSA algorithm.

In Chapter 1, I briefly described the seismic data processing sequences in reflection seismology. Different types of seismic noise are described and different kinds of seismic noise attenuation methods were reviewed. I also reviewed methods for seismic data reconstruction. In Chapter 2, I reviewed concepts in multivariate statistics and linear algebra. The principal component analysis, singular value decomposition and eigendecomposition are described and their relationships are discussed. I described the algorithm of singular spectrum analysis for time series analysis. It is applied to the Southern Oscillation Index (SOI). The f - x SSA for seismic random noise attenuation is shown in this chapter as well. It is an alternative to the f - x deconvolution for random seismic noise attenuation and it has the advantage of preserving the amplitudes of seismic signals. I have recognize that SSA cannot cope with erratic noise and consequently chapter 3 gives a overview of the robust statistics with an emphasis on the M-estimators method. Loss functions other than the quadratic function (ℓ_2 norm) were described and I proposed a robust singular spectrum analysis method for Gaussian and non-Gaussian seismic noise attenuation that utilize robust loss functions. The TSVD in traditional SSA is replaced with the robust low rank approximation that is based on the M-estimate method. The biweight function was chosen as the loss function for our algorithm and iteratively reweighed least-squares and alternating minimization was used for numerically computing the robust factorization. Both

synthetic and field data examples show the superiority of the proposed robust SSA over the traditional SSA and f - x deconvolution for erratic seismic noise attenuation. Moreover, the robust SSA inherits the merit of traditional SSA that preserves the amplitude of the original signal. In Chapter 4, I proposed an algorithm for simultaneously removing Gaussian and non-Gaussian noise and interpolating missing traces. The recovering of low-rank matrix from incompletely observed and Gaussian and impulsive noise corrupted data matrix is solved through a convex optimization program. It minimizes a weighted combination of nuclear-norm, ℓ_1 norm and Frobenius norm. The augmented Lagrangian method is applied for the optimization. Preliminary synthetic examples are given to evaluate the performance of the proposed algorithm.

I conclude that incorporating robust statistics in reduced-rank (SSA) noise attenuation algorithms enables us to design algorithms that are resistant to outliers and erratic noise. This idea is important for processing land and marine seismic data that are often corrupted by noise that does not obey the Gaussian distribution.

There are several possible directions for future work: Extend the proposed robust SSA to the multidimensional case and improve the computational efficiency of the proposed robust algorithm via accelerating the robust low rank approximation step.

Bibliography

- Abma, R. and J. Claerbout. “Lateral prediction for noise attenuation by t - x and f - x techniques.” *Geophysics* 60 (1995): 1887–1896.
- Abma, R. and N. Kabir. “3D interpolation of irregular data with a POCS algorithm.” *Geophysics* 71 (2006): E91–E97.
- Al-Yahya, K. “Application of the partial Karhunen-Loeve transform to suppress random noise in seismic sections.” *Geophysical Prospecting* 39 (1991): 77–93.
- Allen, M. and L. Smith. “Monte Carlo SSA: Detecting irregular oscillations in the Presence of Colored Noise.” *Journal of Climate* 9 (1996).
- Anderson, R. and G. McMechan. “Automatic editing of noisy seismic data.” *Geophysical Prospecting* 37 (1989): 875–892.
- Andrews, H. and B. Hunt. *Digital image restoration*. Prentice-Hall signal processing series. Prentice-Hall, 1977.
- Beaton, A. and J. Tukey. “The Fitting of Power Series, Meaning Polynomials, Illustrated on Band-Spectroscopic Data.” *Technometrics* 16 (1974): pp. 147–185.
- Bekara, M. and M. van der Baan. “High-amplitude noise detection by the expectation-maximization algorithm with application to swell-noise attenuation.” *Geophysics* 75 (2010): V39–V49.
- Berni, A. “Automatic surgical blanking of burst noise in marine seismic data.” *57th Annual International Meeting, SEG, Expanded Abstracts* (1987): 477–478.
- Bertero, M. and E. Pike. “Resolution in Diffraction-limited Imaging, a Singular Value Analysis.” *Optica Acta: International Journal of Optics* 29 (1982): 727–746.
- Bertsekas, D. *Constrained optimization and Lagrange multiplier methods*. Athena Scientific, 1982.

- Brandwood, D. "A complex gradient operator and its application in adaptive array theory." *Communications, Radar and Signal Processing, IEE Proceedings F* 130 (1983): 11–16.
- Broomhead, D. and G. King. "Extracting qualitative dynamics from experimental data." *Physica D: Nonlinear Phenomena* 20 (1986): 217 – 236.
- Broomhead, D. and G. King. "On the qualitative analysis of experimental dynamical systems." *Nonlinear Phenomena and Chaos*. Ed. S. Sarkar. Bristol, England: Adam Hilger, 1986. 113–144.
- Bube, K. and R. Langan. "Hybrid minimization with applications to tomography." *Geophysics* 62 (1997): 1183–1195.
- Butler, K. and R. Russell. "Subtraction of powerline harmonics from geophysical records." *Geophysics* 58 (1993): 898–903.
- Butler, K. and R. Russell. "Cancellation of multiple harmonic noise series in geophysical records." *Geophysics* 68 (2003): 1083–1090.
- Cadzow, J. "Signal enhancement-a composite property mapping algorithm." *Acoustics, Speech and Signal Processing, IEEE Transactions on* 36 (1988): 49–62.
- Cai, J., E. Candès, and Z. Shen. "A Singular Value Thresholding Algorithm for Matrix Completion." *arXiv preprint arXiv:0810.3286* (2008).
- Cambois, G. and J. Frelet. "Can we surgically remove swell noise?." *65th Annual International Meeting, SEG, Expanded Abstracts* (1995): 1381–1384.
- Canales, L. "Random noise reduction." *54th Annual International Meeting, SEG, Expanded Abstracts* (1984): 525–527.
- Candès, E., X. Li, Y. Ma, and J. Wright. "Robust Principal Component Analysis?." *CoRR* abs/0912.3599 (2009).
- Candès, E. and Y. Plan. "Matrix Completion With Noise." *CoRR* abs/0903.3131 (2009).
- Candès, E. and B. Recht. "Exact Matrix Completion via Convex Optimization." *Foundations of Computational Mathematics* 9 (2009): 717–772.
- Candès, E., M. Wakin, and S. Boyd. "Enhancing Sparsity by Reweighted ℓ_1 Minimization." *Journal of Fourier Analysis and Applications* 14 (2008): 877–905.
- Cary, P. and C. Zhang. "Ground roll attenuation with adaptive eigenimage filtering." *79th Annual International Meeting, SEG, Expanded Abstracts* (2009): 3302–3306.

- Chave, A., D. Thomson, and M. Ander. "On the robust estimation of power spectra, coherences, and transfer functions." *Journal of Geophysical Research: Solid Earth* 92 (1987): 633–648.
- Chen, S., D. Donoho, and M. Saunders. "Atomic Decomposition by Basis Pursuit." *SIAM Journal on Scientific Computing* 20 (1998): 33–61.
- Chiu, S. "Coherent and random noise attenuation via multichannel singular spectrum analysis in the randomized domain." *Geophysical Prospecting* 61 (2013): 1–9.
- Chiu, S. and J. Howell. "Attenuation of coherent noise using localized-adaptive eigenimage filter." *78th Annual International Meeting, SEG, Expanded Abstracts* (2008): 2541–2545.
- Claerbout, J. and F. Muir. "Robust modeling with erratic data." *Geophysics* 38 (1973): 826–844.
- Darche, G. "Spatial interpolation using a fast parabolic transform." (1990): 1647–1650.
- Torre, F. De la and M. Black. "A Framework for Robust Subspace Learning." *International Journal of Computer Vision* 54 (2003): 117–142.
- de Prony, G. "Essai expérimental et analytique sur les lois de la dilatabilité des fluides élastiques et sur celles de la force expansive de la vapeur de l'eau et de la vapeur de l'alcool à différentes températures." *J de l'Ecole Polytechnique* 1(2) (1795): 24–76.
- Dondurur, D. and H. Karstl. "Swell Noise Suppression by Wiener Prediction Filter." *Journal of Applied Geophysics* 80 (2012): 91 – 100.
- Dragoset, B. "Geophysical applications of adaptive-noise cancellation." *65th Annual International Meeting, SEG, Expanded Abstracts* (1995): 1389–1392.
- Eckart, C. and G. Young. "The approximation of one matrix by another of lower rank." 10.1007/BF02288367. *Psychometrika* 1 (1936): 211–218.
- Elboth, T., I. Presterud, and D. Hermansen. "Time-frequency seismic data de-noising." *Geophysical Prospecting* 58 (2010): 441–453.
- Elsner, J. and A. Tsonis. *Singular Spectrum Analysis: A New Tool in Time Series Analysis*. Plenum Press, 1996.
- Elston, S. "Use of robust estimators in multichannel stacking." *60th Annual International Meeting, SEG, Expanded Abstracts* (1990): 1693–1696.
- Fraedrich, K. "Estimating the Dimensions of Weather and Climate Attractors." *Journal of the Atmospheric Sciences* 43 (1986): 419–432.

- Freire, S. and T. Ulrych. “Application of singular value decomposition to vertical seismic profiling.” *Geophysics* 53 (1988): 778–785.
- Gabriel, K. and S. Zamir. “Lower Rank Approximation of Matrices by Least Squares with Any Choice of Weights.” *Technometrics* 21 (1979): 489–498.
- Gao, J., M. Sacchi, and X. Chen. “A fast reduced-rank interpolation method for prestack seismic volumes that depend on four spatial dimensions.” *Geophysics* 78 (2013): V21–V30.
- Ghil, M., M. Allen, M. Dettinger, K. Ide, D. Kondrashov, M. Mann, A. Robertson, A. Saunders, Y. Tian, F. Varadi, and P. Yiou. “Advanced spectral methods for climatic time series.” *Reviews of Geophysics* 40 (2002): 3–1–3–41.
- Golub, G. and C. Van Loan. *Matrix Computations*. Third edition. Johns Hopkins Studies in the Mathematical Sciences. Johns Hopkins University Press, 1996.
- Golyandina, N. and A. Zhigljavsky. *Singular Spectrum Analysis for Time Series*. Springer-Briefs in Statistics. Springer London, Limited, 2013.
- Guittou, A. and W. Symes. “Robust inversion of seismic data using the Huber norm.” *Geophysics* 68 (2003): 1310–1319.
- Gulunay, N. “FXDECOR and complex wiener prediction filter.” *56th Annual International Meeting, SEG, Expanded Abstracts* (1986): 279–281.
- Gulunay, N. “Seismic trace interpolation in the Fourier transform domain.” *Geophysics* 68 (2003): 355–369.
- Halko, N., P. Martinsson, and J. Tropp. “Finding Structure with Randomness: Probabilistic Algorithms for Constructing Approximate Matrix Decompositions.” *SIAM Review* 53 (2011): 217–288.
- Hampel, F., E. Ronchetti, P. Rousseeuw, and W. Stahel. *Robust Statistics: The Approach Based on Influence Functions*. John Wiley & Sons, Inc, 1986.
- Hansen, P. *Rank-Deficient and Discrete Ill-Posed Problems*. Society for Industrial and Applied Mathematics, 1998.
- Harris, P. and R. White. “Improving the performance of f - x prediction filtering at low signal-to-noise ratios.” *Geophysical Prospecting* 45 (1997): 269–302.
- Hemon, CH. and D. Mace. “Use of the Karhunen-Loeve transformation in seismic data processing.” *Geophysical Prospecting* 26 (1978): 600–626.

- Herrmann, F. and G. Hennenfent. "Non-parametric seismic data recovery with curvelet frames." *Geophysical Journal International* 173 (2008): 233–248.
- Holland, P. and R. Welsch. "Robust regression using iteratively reweighted least-squares." *Communications in Statistics - Theory and Methods* 6 (1977): 813–827.
- Hornbostel, S. "Spatial prediction filtering in the t-x and f-x domains." *Geophysics* 56 (1991): 2019–2026.
- Huber, P. "Robust Estimation of a Location Parameter." *The Annals of Mathematical Statistics* 35 (1964): pp. 73–101.
- Huber, P. *Robust Statistics*. John Wiley & Sons, Inc, 1981.
- Johnson, R. and D. Wichern. *Applied multivariate statistical analysis*. Sixth edition. Pearson Prentice-Hall, 2007.
- Jolliffe, I. *Principal Component Analysis*. Second edition. Springer Series in Statistics. Springer, 2010.
- Jones, I. and S. Levy. "Signal-to-noise ratio enhancement in multichannel seismic data via the Karhunen-Loeve Transform." *Geophysical Prospecting* 35 (1987): 12–32.
- Kaplan, S., M. Naghizadeh, and M. Sacchi. "Data reconstruction with shot-profile least-squares migration." *Geophysics* 75 (2010): WB121–WB136.
- Karhunen, K. "Ueber lineare Methoden in der Wahrscheinlichkeitsrechnung." *Annales Academiae scientiarum Fennicae. Series A* 137 (1947).
- Kreimer, N. and M. Sacchi. "A tensor higher-order singular value decomposition for prestack seismic data noise reduction and interpolation." *Geophysics* 77 (2012): V113–V122.
- Lin, Z., M. Chen, and Y. Ma. "The Augmented Lagrange Multiplier Method for Exact Recovery of Corrupted Low-Rank Matrices." *ArXiv e-prints* (sep 2010).
- Linville, A. and R. Meek. "Canceling stationary sinusoidal noise." *Geophysics* 57 (1992): 1493–1501.
- Liu, B. and M. Sacchi. "Minimum weighted norm interpolation of seismic records." *Geophysics* 69 (2004): 1560–1568.
- Liu, X. "Ground roll supression using the Karhunen-Loeve transform." *Geophysics* 64 (1999): 564–566.
- Loeve, M. "Fonctions alatoires de seconde ordre." *Processus Stochastiques et Mouvement Brownien* (1948).

- Marchisio, G., J. Pendrel, and B. Mattocks. "Applications of full and partial Karhunen-Loeve transformation to geophysical image enhancement." *58th Annual International Meeting, SEG, Expanded Abstracts* (1988): 1266–1269.
- Mari, J. and F. Glangeaud. "Spectral Matrix Filtering Applied to VSP Processing." *Oil & Gas Science and Technology - Rev. IFP* 45 (1990): 417–434.
- Maronna, R., R. Martin, and V. Yohai. *Robust Statistics*. John Wiley & Sons, Inc, 2006.
- Maronna, R. and V. Yohai. "Robust Low-Rank Approximation of Data Matrices With Elementwise Contamination." *Technometrics* 50 (2008): 295–304.
- Mars, J., F. Glangeaud, J. Lacoume, J. Fourmann, and S. Spitz. "Separation of seismic waves." *57th Annual International Meeting, SEG, Expanded Abstracts* (1987): 489–492.
- Mavko, G. "Spectra-consistent automatic noise editing." *58th Annual International Meeting, SEG, Expanded Abstracts* (1988): 1275–1277.
- Mayne, W. "Common reflection point horizontal data stacking techniques." *Geophysics* 27 (1962): 927–938.
- Nagarajappa, N. "Coherent noise estimation by adaptive Hankel matrix rank reduction." *82nd Annual International Meeting, SEG, Expanded Abstracts* (2012): 1–5.
- Naghizadeh, M. and M. Sacchi. "Multidimensional de-aliased Cadzow reconstruction of seismic records." *Geophysics* 78 (2013): A1–A5.
- Neff, D. and S. Wyatt. "Noise suppression by the radial amplitude-slope rejection method." *Geophysics* 51 (1986): 844–850.
- Oropeza, V. and M. Sacchi. "Application of singular spectrum analysis to ground roll attenuation." *CSPG CSEG CWLS Convention* (2010).
- Oropeza, V. and M. Sacchi. "Simultaneous seismic data denoising and reconstruction via multichannel singular spectrum analysis." *Geophysics* 76 (2011): V25–V32.
- Papoulis, A. and S. Pillai. *Probability, Random Variables And Stochastic Processes*. Fourth edition. McGraw-Hill series in electrical engineering. McGraw-Hill, 2002.
- Rasmusson, E., X. Wang, and C. Ropelewski. "The biennial component of ENSO variability." *Journal of Marine Systems* 1 (1990): 71 – 96.
- Sacchi, M. "FX Singular Spectrum Analysis." *CSPG CSEG CWLS CONVENTION* (2009).
- Sacchi, M. and H. Kuehl. "ARMA formulation of FX prediction error filters and projection filters." *Journal of Seismic Exploration* 3 (2001): 185–197.

- Sacchi, M., T. Ulrych, and C. Walker. "Interpolation and extrapolation using a high-resolution discrete Fourier transform." *Signal Processing, IEEE Transactions on* 46 (1998): 31–38.
- Sardy, S. "Minimax threshold for denoising complex signals with Waveshrink." *Signal Processing, IEEE Transactions on* 48 (apr 2000): 1023–1028.
- Scales, J. and A. Gersztenkorn. "Robust methods in inverse theory." *Inverse Problems* 4 (1988): 1071.
- Scales, J., A. Gersztenkorn, and S. Treitel. "Fast l_p solution of large, sparse, linear systems: Application to seismic travel time tomography." *Journal of Computational Physics* 75 (1988): 314–333.
- Schonewille, M., A. Vigner, and A. Ryder. "Swell-noise attenuation using an iterative FX prediction filtering approach." *78th Annual International Meeting, SEG, Expanded Abstracts* (2008): 2647–2651.
- Simon, H. and H. Zha. "Low-Rank Matrix Approximation Using the Lanczos Bidiagonalization Process with Applications." *SIAM Journal on Scientific Computing* 21 (2000): 2257–2274.
- Soubaras, R. "Signal-preserving random noise attenuation by the f - x projection." *64th Annual International Meeting, SEG, Expanded Abstracts* (1994): 1576–1579.
- Soubaras, R. "Prestack random and impulsive noise attenuation by f - x projection filtering." *65th Annual International Meeting, SEG, Expanded Abstracts* (1995): 711–714.
- Soubaras, R. "Spatial interpolation of aliased seismic data." (1997): 1167–1170.
- Spitz, S. "Seismic trace interpolation in the F-X domain." *Geophysics* 56 (1991): 785–794.
- Stolt, R. "Seismic data mapping and reconstruction." *Geophysics* 67 (2002): 890–908.
- Strang, G. *Introduction to Linear Algebra*. Wellesley-Cambridge Press, 1993.
- Strang, G. *Linear Algebra and Its Applications*. Fourth edition. Thomson Brooks/Cole, 2006.
- Takens, F. "Detecting strange attractors in turbulence." *Dynamical Systems and Turbulence, Warwick 1980*. . Lecture Notes in Mathematics. Springer Berlin Heidelberg, 1981. 366–381.
- Tao, M. and X. Yuan. "Recovering Low-Rank and Sparse Components of Matrices from Incomplete and Noisy Observations." *SIAM Journal on Optimization* 21 (2011): 57–81.

- Taylor, H., S. Banks, and J. McCoy. "Deconvolution with the ℓ_1 norm." *Geophysics* 44 (1979): 39–52.
- Trad, D. "Interpolation and multiple attenuation with migration operators." *Geophysics* 68 (2003): 2043–2054.
- Trad, D., T. Ulrych, and M. Sacchi. "Accurate interpolation with highresolution timevariant Radon transforms." *Geophysics* 67 (2002): 644–656.
- Trickett, S. "F-x eigenimage noise suppression." *72nd Annual International Meeting, SEG, Expanded Abstracts* (2002): 2166–2169.
- Trickett, S. "F-xy eigenimage noise suppression." *Geophysics* 68 (2003): 751–759.
- Trickett, S. "Maximum-likelihood estimation stacking." *77th Annual International Meeting, SEG, Expanded Abstracts* (2007): 2640–2643.
- Trickett, S. "F-x Cadzow noise suppression." *78th Annual International Meeting, SEG, Expanded Abstracts* (2008): 2586–2590.
- Trickett, S. and L. Burroughs. "Prestack rankreducing noise suppression: Theory." *79th Annual International Meeting, SEG, Expanded Abstracts* (2009): 3332–3336.
- Trickett, S., L. Burroughs, and A. Milton. "Robust rank-reduction filtering for erratic noise." *82nd Annual International Meeting, SEG, Expanded Abstracts* (2012): 1–5.
- Trickett, S., L. Burroughs, A. Milton, L. Walton, and R. Dack. "Rank-reduction-based trace interpolation." *80th Annual International Meeting, SEG, Expanded Abstracts* (2010): 3829–3833.
- Tufts, D. and R. Kumaresan. "Estimation of frequencies of multiple sinusoids: Making linear prediction perform like maximum likelihood." *Proceedings of the IEEE* 70 (1982): 975–989.
- Ulrych, T. and R. Clayton. "Time series modelling and maximum entropy." *Physics of the Earth and Planetary Interiors* 12 (1976): 188 – 200.
- Ulrych, T., S. Freire, and P. Siston. "Eigenimage processing of seismic sections." *58th Annual International Meeting, SEG, Expanded Abstracts* (1988): 1261–1265.
- Ulrych, T. and M. Sacchi. *Information-Based Inversion and Processing with Applications*. Handbook of Geophysical Exploration: Seismic Exploration. Elsevier Science, 2005.
- Ulrych, T., M. Sacchi, and J. Graul. "Signal and noise separation: Art and science." *Geophysics* 64 (1999): 1648–1656.

- Vautard, R. and M. Ghil. “Singular spectrum analysis in nonlinear dynamics, with applications to paleoclimatic time series.” *Physica D: Nonlinear Phenomena* 35 (1989): 395 – 424.
- Vautard, R., P. Yiou, and M. Ghil. “Singular-spectrum analysis: A toolkit for short, noisy chaotic signals.” *Physica D: Nonlinear Phenomena* 58 (1992): 95 – 126.
- Verboon, P. and W. Heiser. “Resistant lower rank approximation of matrices by iterative majorization.” *Computational Statistics & Data Analysis* 18 (1994): 457 – 467.
- Watt, T. and J. Bednar. “Role of the alpha-trimmed mean in combining and analyzing seismic commondepthpoint gathers.” *53rd Annual International Meeting, SEG, Expanded Abstracts* (1983): 276–277.
- Widrow, B., P. Mantey, L. Griffiths, and B. Goode. “Adaptive antenna systems.” *Proceedings of the IEEE* 55 (1967): 2143–2159.
- Yilmaz, Oz. *Seismic Data Analysis: Processing, Inversion, and Interpretation of Seismic Data*. Second edition. Society of Exploration Geophysicists, 2001.
- Yuan, X. and J. Yang. “Sparse and low-rank matrix decomposition via alternating direction methods.” (2009).
- Zhou, Z., X. Li, J. Wright, E. Candès, and Y. Ma. “Stable Principal Component Pursuit.” *CoRR* abs/1001.2363 (2010).

APPENDIX A

Gradient in Complex Domain

Here, I describe how to use the partial complex derivative to compute the weighting function of the cost function (3.75):

$$E(\mathbf{U}, \mathbf{V}) = \sum_{i=1}^m \sum_{j=1}^n \rho \left(\frac{m_{ij} - \sum_{q=1}^K u_{iq} v_{jq}^*}{\sigma} \right) = \sum_{i=1}^m \sum_{j=1}^n \rho \left(\frac{r_{ij}}{\sigma} \right). \quad (\text{A.1})$$

If the matrix \mathbf{V} is fixed, E is a function of \mathbf{U} . Similarly, E is a function of \mathbf{V} if \mathbf{U} is fixed. However, even though \mathbf{V} is fixed, E is not a complex analytic function with respect to \mathbf{U} . The complex derivative does not exist. By using Wirtinger's Calculus (Brandwood, 1983), we can regard \mathbf{U} and \mathbf{U}^* as independent variables. Either setting the partial derivative $\frac{\partial E}{\partial \mathbf{U}}$ or $\frac{\partial E}{\partial \mathbf{U}^*}$ to zero lead to stationary points. Usually, $\frac{\partial E}{\partial \mathbf{U}^*}$ is preferred because it gives the direction where the cost function E has the maximum rate of change with respect to \mathbf{U} .

(Brandwood, 1983).

$$\begin{aligned}
\frac{\partial E}{\partial u_{ab}^*} &= \sum_{i=1}^m \sum_{j=1}^n \frac{\partial \rho \left(\frac{r_{ij}}{\sigma}, \frac{r_{ij}^*}{\sigma} \right)}{\partial u_{ab}^*} = \sum_{j=1}^n \frac{\partial \rho \left(\frac{r_{aj}}{\sigma}, \frac{r_{aj}^*}{\sigma} \right)}{\partial u_{ab}^*} \\
&= \sum_{j=1}^n \left(\frac{\partial \rho \left(\frac{r_{aj}}{\sigma}, \frac{r_{aj}^*}{\sigma} \right)}{\partial r_{aj}} \frac{\partial r_{aj}}{\partial u_{ab}^*} + \frac{\partial \rho \left(\frac{r_{aj}}{\sigma}, \frac{r_{aj}^*}{\sigma} \right)}{\partial r_{aj}^*} \frac{\partial r_{aj}^*}{\partial u_{ab}^*} \right) \\
&= \sum_{j=1}^n \frac{\partial \rho \left(\frac{r_{aj}}{\sigma}, \frac{r_{aj}^*}{\sigma} \right)}{\partial r_{aj}^*} \frac{\partial r_{aj}^*}{\partial u_{ab}^*} = - \sum_{j=1}^n \frac{\partial \rho \left(\frac{r_{aj}}{\sigma} \right)}{\partial r_{aj}^*} v_{jb} \\
&= - \sum_{j=1}^n \frac{\partial \rho \left(\frac{r_{aj}}{\sigma} \right)}{\partial r_{aj}^*} \frac{1}{r_{aj}} r_{aj} v_{jb} \\
&= - \frac{1}{\sigma^2} \sum_{j=1}^n w \left(\frac{r_{aj}}{\sigma} \right) r_{aj} v_{jb},
\end{aligned} \tag{A.2}$$

where $w(x) = \frac{\partial \rho(x)}{\partial x^*} \frac{1}{x}$ with $x = \frac{r_{aj}}{\sigma}$ is the weighting function that is different from real value case. In the above equations, ρ is not an analytic function of r_{aj} or r_{aj}^* therefore, we applied the chain rule to the complex partial derivative of r_{aj} and r_{aj}^* . Due to the relationship $\frac{\partial |x|}{\partial x^*} = \frac{1}{2} \frac{x}{|x|}$, we have that $w(x) = \frac{\partial \rho(x)}{\partial x^*} \frac{1}{x} = \frac{\partial \rho(x)}{\partial x} \frac{1}{x^*} = \frac{1}{2} \frac{\partial \rho(x)}{\partial |x|} \frac{1}{|x|}$.

Similarly, we can compute $\frac{\partial E}{\partial v^*}$

$$\begin{aligned}
\frac{\partial E}{\partial v_{cd}^*} &= \sum_{i=1}^m \sum_{j=1}^n \frac{\partial \rho \left(\frac{r_{ij}}{\sigma}, \frac{r_{ij}^*}{\sigma} \right)}{\partial v_{cd}^*} = \sum_{i=1}^m \frac{\partial \rho \left(\frac{r_{ic}}{\sigma}, \frac{r_{ic}^*}{\sigma} \right)}{\partial v_{cd}^*} \\
&= \sum_{i=1}^m \left(\frac{\partial \rho \left(\frac{r_{ic}}{\sigma}, \frac{r_{ic}^*}{\sigma} \right)}{\partial r_{ic}} \frac{\partial r_{ic}}{\partial v_{cd}^*} + \frac{\partial \rho \left(\frac{r_{ic}}{\sigma}, \frac{r_{ic}^*}{\sigma} \right)}{\partial r_{ic}^*} \frac{\partial r_{ic}^*}{\partial v_{cd}^*} \right) \\
&= \sum_{i=1}^m \frac{\partial \rho \left(\frac{r_{ic}}{\sigma} \right)}{\partial r_{ic}} \frac{\partial r_{ic}}{\partial v_{cd}^*} = \sum_{i=1}^m \frac{\partial \rho \left(\frac{r_{ic}}{\sigma} \right)}{\partial r_{ic}} (-u_{id}) \\
&= - \sum_{i=1}^m \frac{\partial \rho \left(\frac{r_{ic}}{\sigma} \right)}{\partial r_{ic}} \frac{1}{r_{ic}^*} r_{ic}^* u_{id} \\
&= - \frac{1}{\sigma^2} \sum_{i=1}^m w \left(\frac{r_{ic}}{\sigma} \right) r_{ic}^* u_{id},
\end{aligned} \tag{A.3}$$

where $w(x) = \frac{\partial \rho(x)}{\partial x} \frac{1}{x^*} = \frac{\partial \rho(x)}{\partial x^*} \frac{1}{x} = \frac{1}{2} \frac{\partial \rho(x)}{\partial |x|} \frac{1}{|x|}$ with $x = \frac{r_{ic}}{\sigma}$.